Fully Coupled Fluid-Structure Algorithms for Aeroelasticity and Forced Vibration Induced Flutter

Applications to a Compressor Cascade

Pénélope Leyland* **Volker Carstens****
Frederic Blom* **Tiana Tefy ****

* *Département de Génie Mécanique, Ecole Polytechnique Fédérale de Lausanne, CH-1015 Lausanne, Suisse*
penelope.leyland@epfl.ch

** *Deutsches Zentrum für Luft- und Raumfahrt, DLR, Institute of Aeroelasticity, Bunsenstrasse 10, D-37073 Göttingen, Allemagne*
Volker.Carstens@dlr.de

ABSTRACT. *Algorithms for Fluid-Structure Coupling techniques are investigated in the time domain. The accurate prediction of the interaction requires consistency of the interface boundary conditions with the time levels of integration of the fluid and the structure equations. If staggered algorithms are used, the time delay causes non-physical energy dissipation in the system which modifies the calculated aeroelastic behaviour. In order to be compatible, the equations must be integrated simultaneously and implicitly. These techniques are tested on a standard aeroelastic airfoil problem, and then applied to the direct coupling of an assembly of 20 compressor blades performing torsional vibrations.*

RÉSUMÉ. *Cet article concerne des algorithmes de couplage fluide-structure pour des études d'aéroélasticité dans le domaine temporel. Les considérations de la conservation énergétique du système couplé amènent aux méthodes fortement couplées où le calcul de la déformation de la structure et de l'aérodynamique du fluide est évalué au même niveau de temps, pour éviter l'introduction de décalage dans le système. Ceci nécessite l'introduction d'une consistance temporelle des conditions de l'interface. Les techniques sont appliquées au comportement aéroélastique d'un profil NACA et à l'analyse de flottement d'une cascade de compresseur.*

KEYWORDS: *Coupling Algorithms, Flutter, Interaction, Flow, Structure, Energy, Aeroelasticity, Boundary Conditions, Consistency in time.*

MOTS-CLÉS : *Algorithmes de couplage, Flottement, Interaction, Fluide, Structure, Energie, Conditions limites, Consistance en temps, Aeroélasticité.*

1. Introduction

Simulating the aeroelastic behaviour of realistic configurations such as airplane wing assemblies or turbomachinery components is now within the capabilities of computer power and numerical methods. However, the process can become an extremely long and costly enterprise, especially when precise methods are demanded. Often it is sufficient to use frequency domain techniques based on linearised equations and a linear relationship between the aerodynamic loads and the structural deformation. These methods fail when non-linear effects are important such as vibrating shocks as in transonic regimes or non linearities in the structure properties, then time domain methods are necessary. The fluid and the structural equations can be solved separately or together, in each case the reaction of the fluid from the deforming structure and vice versa takes place at the interface between the two. For example, an aeroelastic fluid-structure interaction computation requires that the airloads induced by the flow on the solid are translated via a boundary condition as the external forces for the structural mechanics calculation, which in turns leads to a deformation of the structure which needs to be accounted for in the fluid dynamics simulation. In general, the geometrical representation and the numerical techniques used in the fluid and structural mechanics computations are not the same; as a result the coupling of these two simulation methods requires algorithms that maintain energy transfer conservation, time consistency and accuracy in order to remain representative.

Algorithms for fluid-structure coupling in the time domain can be considered as being staggered: the fluid and the structure evolve separately, and updating is performed at specific moments. Various degrees of subcycling can be performed within the individual steps. These methods introduce a time delay, which translates as non-physical energy dissipation. The impact of these errors is less important if the time stepping procedure uses small time steps, as is the case with explicit time marching algorithms. However, to be both accurate and competitive, it is clear that any numerical technique for fluid-structure coupling should try to use techniques with the highest value of time stepping as possible, and evaluate the different parts, fluid and structure such in a simultaneous and implicit way. Particular interest has recently been given to fully coupled methods, where the coupling takes place at the same time level. These methods are discussed here and tested first on a standard aeroelastic airfoil problem, for weakly unstable and also unstable conditions where the calculations are extended to capture a limit cycle behaviour, and then applied to the direct coupling of an assembly of 20 compressor blades performing torsional vibrations. The aeroelastic stability of this cascade is investigated by forced vibration calculations as well as direct coupled simulations.

The aerodynamics are simulated with finite volume techniques on structured and unstructured meshes, using implicit time integration. The structural models are integrated with the Newmark algorithm. An ALE method can be used for the moving and deforming boundaries. The mesh deformation is taken into account using a dynamic spring analogy or using interactive grid generation with transfinite interpolation for the updated mesh locations. It is possible to compensate for the three dimensionality

of a real annular compressor cascade by introducing the so-called streamtube contraction correction, which simulates the blocking of the flow which is directed radially outwards by the existence of interaction between the channel flow and the hub. This acts like an axisymmetric term in the fluid equations.

Whenever there can be no confusion, the evolution of the geometry is inherently contained in the formulae, and the suffixes $_f$ and $_s$ denoting respectively *fluid* and *structure* are dropped.

2. Basic Governing Equations

In this paper fluid-structure interaction problems are studied from the point of view of aeroelasticity.

The fluid movement exerts aerodynamic forces on the structure which reacts and in turn forces the flow to evolve at the interface with an interface velocity represented by $\vec{V_S}$. This produces the coupling effect. The boundary is time dependent, which means that within the Eulerian frame of reference of the fluid, the domain in which the fluid evolves deforms in time. The consequent discretisation of the governing equations for the fluid takes into account this effect, as does also the spatial discretisation (the computational fluid mesh which now is a moving and deforming mesh). The fluid equations on a moving domain are given here using the Arbitrary Lagrange Euler formulation, [DON 82]. There are several techniques to describe the deforming mesh, here two different techniques are used. The first treats the mesh as an elastic system, the mesh segments being replaced by springs of various complexity, the second method exploits the fact that the geometries are identical airfoils or blades, and using mesh re-generation with transfinite interpolation and elliptic smoothing. It has been shown in [BLO 98a],[CAR 88],[GRÜ 96] that these are in fact identical methods when linear elastic springs are used in the mesh deformation formulation.

The so-called coupled trio fluid-structure-mesh hence forms a coupled mechanical system. The coupling in the time domain is obtained by solving simultaneously the systems of the structural and the fluid equations.

The equations of motion for discrete structures can be written in the following matrix form :

$$[\mathbf{M}]\{\vec{\ddot{q}_s}\} + [\mathbf{D}]\{\vec{\dot{q}_s}\} + [\mathbf{K}]\{\vec{q_s}\} = \{\vec{F}\} \quad \text{for the structure;} \qquad [1]$$

where the vector $\vec{q_s}$ contains the physical or generalised displacements belonging to the different degrees of freedom, and where $[\mathbf{M}]$, $[\mathbf{D}]$, $[\mathbf{K}]$ denote the mass, damping and stiffness matrices respectively.

For aeroelastic investigations, the right-hand side vector $\{\vec{F}\}$ represents the physical or generalised aerodynamic forces acting on the system. This vector is usually a

nonlinear function of the fluid state vector and the displacement vector together with its time derivatives :

$$\vec{F} = \vec{F}(\vec{\mathbf{W}}, \vec{q}, \dot{\vec{q}}, \ddot{\vec{q}}) \qquad [2]$$

The fluid state vector $\vec{\mathbf{W}}$ is determined from the solution of the system of the governing fluid equations, which can be expressed in a semi-discrete form as :

$$\frac{d\vec{\mathbf{W}}}{dt} = \vec{R}(\vec{\mathbf{W}}, \vec{q}, \dot{\vec{q}}, \ddot{\vec{q}}); \qquad [3]$$

where the so-called residual vector $\vec{R}$ contains the discretised spatial derivatives of the mass, momentum and energy fluxes of the flow. This residual is again a non-linear function of its arguments.

Writing the fluid system in conservation form with conservative variables, and the state vector $\vec{\mathbf{W}} = (\rho, \rho\vec{u_f}, \rho E)^T$, of density ρ, momentum $\rho\vec{u_f}$, and total energy ρE, in an Eulerian frame of reference for a domain $\Omega(t)$ of boundaries $\partial\Omega(t)$:

$$\frac{\partial}{\partial t}\int_{\Omega(t)} \vec{\mathbf{W}} d\Omega + \int_{\partial\Omega(t)} \mathcal{F}(\vec{\mathbf{W}}) \cdot \vec{n} d\sigma = 0 \quad \text{for the fluid.} \qquad [4]$$

Then the residual $\vec{R}$ will be given by the numerical flux function approximating the second term.

This system is completed by the boundary conditions at the exterior of the fluid domain, $\partial\Omega_\infty(t)$ and at the interface $\Gamma(t)$.

Finally, an elasticity equation for the mesh deformation can be considered :

$$[\mathbf{M_i}]\{\ddot{\vec{\xi}}_i\} + [\mathbf{D_i}]\{\dot{\vec{\xi}}_i\} + [\mathbf{K_i}]\{\vec{\xi}_i\} = \{\vec{F}_3\} \quad \text{for the elastic mesh,} \qquad [5]$$

where ξ_i denotes the mesh segment or vertex displacements.

This last system can in fact be incorporated directly into the detailed versions of the coupled equations [1],[3], as the discretisation domain follows the surface of the vibrating solid boundary. Therefore, the time dependence of the fluid mesh is the same as that for the blade motion. In the ALE formulation the moving co-ordinates are included within the geometrical discretisation, a mesh speed is introduced. A consistent solid interface speed must be introduced, see section 5.3. When the interface velocities are linear in time the trapezoidal rule is used. Then the calculation of the normal vectors in [3] at $\Gamma(t)$ is taken at $t + \frac{1}{2}\Delta t$ to satisfy the Geometrical Conservation Law.

Detailed analysis on the treatment of the trio treatment has been given in particular by [FAR 95],[FAR 98d],[FAR 98a],[FAR 00]. Here we will formulate the coupled problem as a fluid-structure one. The mesh movement is thus automatically accounted

for during the ALE formulation and the time consistent boundary condition at the interface.

The combination of the equations [1], [3], into one single system is achieved by rewriting [1], as a first order system. Introducing the new variables :

$$\vec{x_1} = \vec{q}, \quad \vec{x_2} = \dot{\vec{q}}, \quad \vec{\mathbf{x}} = \{\vec{x_1}, \vec{x_2}\}^T, \tag{6}$$

the system of structural equations is now given by

$$\dot{\vec{\mathbf{x}}} = [\mathbf{A}]\,\vec{\mathbf{x}} + \vec{\mathbf{b}}(\vec{\mathbf{W}}, \vec{\mathbf{x}}, \dot{\vec{\mathbf{x}}}), \tag{7}$$

with

$$[\mathbf{A}] = \begin{bmatrix} 0 & \mathbf{I} \\ -[\mathbf{M}]^{-1}[\mathbf{K}] & -[\mathbf{M}]^{-1}[\mathbf{D}] \end{bmatrix}; \quad \vec{\mathbf{b}} = \begin{bmatrix} 0 \\ -[\mathbf{M}]^{-1}\vec{F}(\vec{\mathbf{W}}, \vec{\mathbf{x}}, \dot{\vec{\mathbf{x}}}) \end{bmatrix} \tag{8}$$

Collecting [7] and [8], into one equation, we finally obtain the nonlinear system

$$\frac{d}{dt}\begin{bmatrix} \vec{\mathbf{x}} \\ \vec{\mathbf{W}} \end{bmatrix} = \begin{bmatrix} [\mathbf{A}]\vec{\mathbf{x}} + \vec{\mathbf{b}}(\vec{\mathbf{W}}, \vec{\mathbf{x}}, \dot{\vec{\mathbf{x}}}) \\ \vec{\mathbf{R}}(\vec{\mathbf{W}}, \vec{\mathbf{x}}, \dot{\vec{\mathbf{x}}}) \end{bmatrix} \tag{9}$$

In order to solve the system [9] in the time domain, time accurate explicit integration methods are the simplest to use, however they are computationally inefficient as the time step, and the associated stability are restricted. Indeed, the fluid and structure are integrated in time by taking the same time step Δt_{fsi} for the fluid as well as the structure. The size of this time step is determined by

$$\Delta t_{fsi} = min(\Delta t_f, \Delta t_s), \tag{10}$$

where the structural time step Δt_s is restricted by the structural stability or accuracy requirements. The fluid time step Δt_f is restricted by a CFL like condition. The corresponding stability domain of the explicit iterative method can be particularly reduced, and truncation errors can accumulate during the solution process in time. Aeroelasticity often requires the calculation of many vibrational cycles in order to evaluate stability and onset of instability. In order to devise efficient, accurate, stable and as will be seen later energy preserving methods, implicit time stepping algorithms are more appropriate to advance the solution of [9]. The simultaneous solution of both the structural and the fluid equations has two important drawbacks :

1. Structure and fluid are integrated on the same time scale, although the characteristic scales for the structural system and for the fluid flow may be completely different.
2. The specific methods of time integration developed for solving either structural dynamics problems or computing unsteady flow can no longer be applied directly.

For these reasons, implicit time-staggered methods have been developed where either the displacement vector $\vec{q_s}$ or the fluid state vector $\vec{\mathbf{W}}$ are predicted at time step $n+1$ while the other quantity, ($\vec{\mathbf{W}}$ or $\vec{q_s}$) is integrated implicitly by its own specific method. This procedure leads to a decoupled updating of the two vectors $\vec{q_s}$ and $\vec{\mathbf{W}}$ and permits the application of different time steps in the individual structure and fluid parts, while the overall time step for advancing $\vec{q_s}$ and $\vec{\mathbf{W}}$ from n to $n+1$ is prescribed. There are many variants and improvements of this basic scheme, with different degrees of prediction, correction and use of intermediate states.

In the following sections, the fluid and structure solvers are detailed, and the coupling algorithms are presented.

3. Fluid Solver - The Euler System on a Moving Domain

The unsteady aerodynamic forces are computed by solving the system of equations for inviscid compressible flow, i.e. the Euler equations. Introducing the Navier-Stokes system increases the physical damping of the system but increases the computational complexity with appropriate turbulence modelling, and the delicate problem of moving shock wave-boundary layer interactions. The global efforts can be reasonably estimated by the inviscid part of the aerodynamic forces and moments.

The moving and deforming structural boundary implies that the fluid equations now need to be written on a moving domain. For this, the Arbitrary Lagrange Euler formulation, [DON 82], is adopted. The computational domain, denoted by Ω, is now also time dependent $\Omega(t)$, and the boundary is denoted by $\partial\Omega(t)$, $\vec{n}$ denotes the outward normal of the domain. This requires that the numerical formulation of the Euler equations be verified for the moving cells of volume $\mathcal{V}_{C_i}$ which discretise the domain $\Omega(t)$. The accuracy of the numerical method in time will now depend on consistency arguments in time also for the geometrical quantities. This is known as the Discrete Geometric Conservation Law, and needs to be enforced when moving meshes are present, [FAR 98a].

The continuous system of the Euler equations on a moving domain are given by [4]. In two spatial dimensions the state vector is $\vec{\mathbf{W}} = (\rho, \rho u, \rho v, \rho E)^T$ and the flux tensor is

$$\mathcal{F} = \left[\begin{array}{cc} \mathcal{F}_1 & \mathcal{F}_2 \end{array} \right] = \left[\begin{array}{ll} \rho U & \rho V \\ \rho U u + p & \rho V u \\ \rho U v & \rho V v + p \\ U(\rho E + p) + x_t p & V(\rho E + p) + y_t p \end{array} \right] \qquad [11]$$

and ρ, u, v, E and p denote the density, velocity in x and y direction, total energy and pressure respectively. The Cartesian relative velocities U and V are defined by

$$U = u - x_t; \quad V = v - y_t,$$

where x_t and y_t are the coordinate velocities in x and y direction respectively. The system is closed by a state equation for perfect gases.

The spatial discretisation of the Euler equations by a finite volume method on $\Omega(t) = \bigcup C_i(t)$, with solid, domain and intersection boundaries $\mathbf{B}$, can be expressed by :

$$\mathbf{B} = \partial C_i(t) \cap \{\partial\Omega(t) \cup \Gamma(t)\}$$

$$\sum_{i=1}^{N} \left[\frac{\partial}{\partial t} \int_{C_i(t)} \vec{\mathbf{W}} d\Omega + \sum_{j \in \upsilon_i} \int_{\partial C_{ij}(t)} \mathcal{F}(\vec{\mathbf{W}}) \cdot \vec{n}_{ij} d\sigma + \int_{\mathbf{B}} \mathcal{F}(\vec{\mathbf{W}}) \cdot \vec{n}_{\mathbf{B}} d\sigma \right] = 0 \quad [12]$$

where $C_i(t)$ denotes the finite volume cells, υ_i denotes the set of adjacent cells for the cell centred at i. ∂C_{ij} denotes the face between the cell centred at i and the neighbouring cell centred at j. The numerical flux is evaluated at these faces, $\mathbf{\Phi}_{ij}$ and is defined as

$$\mathbf{\Phi}_{ij}(\vec{\mathbf{W}}_i, \vec{\mathbf{W}}_j, \vec{n}) \overset{approx.}{=} \int_{\partial C_{ij}(t)} \mathcal{F}(\vec{\mathbf{W}}) \cdot \vec{n}_{ij} d\sigma \quad [13]$$

Since the fully implicit method chosen must not only be temporally but also spatially accurate, it is necessary to choose a numerical flux that is as exactly differentiable as possible for the calculation of the Jacobian matrices. Numerical approximations of the Jacobians have also been analysed in other papers of the present issue. The Van Leer flux vector splitting schemes written on moving meshes have been chosen, as in [BAT 90]. This flux is then made second-order accurate in space using the MUSCL interpolation, and a suitable limiter such as min-mod or superbee.

3.1. *Mesh Movement*

The meshes are taken to be either structured or unstructured, as illustrated in the Figure 1. Two methods are used here to allow the discretisation domain to move with the deforming solid boundary: the spring analogy which consists of replacing the mesh by fictitious springs, and an automatic mesh regeneration after each time step which is achieved by transfinite interpolation and elliptic smoothing. This method is applied by Grüber and Carstens [GRÜ 96] for forced vibrations and by Carstens and Belz [CAR 00] for free vibrations of cascades. In fact, using an analogy with molecular theory the spring analogy can be formulated to be equivalent to elliptic grid generation, [BLO 98a]. The method of re-meshing with transfinite interpolation is obviously clearer for the structured mesh type.

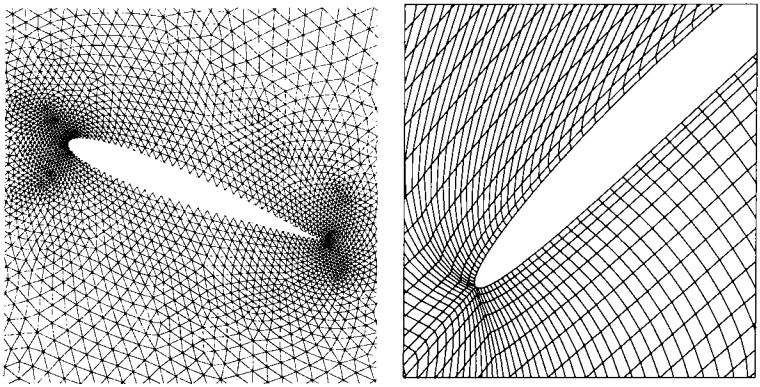

Figure 1. *Typical meshes employed in this paper, an unstructured mesh around a NACA-type profile, that can be adapted dynamically and deformed using a segment stiffened spring analogy; a structured mesh around a typical blade of a turbine cascade which is re-meshed using transfinite interpolation to follow the blade movement*

3.2. *Time Integration*

The Euler equations are integrated by an implicit method. Let $\mathcal{V}$ be the cell area of $C_i(t)$. The indexation of the current cell, "i" is dropped when there is no ambiguity. The time integration can be written as

$$\mathcal{V}^{n+1}\vec{\mathbf{W}}^{n+1} - \mathcal{V}^{n}\vec{\mathbf{W}}^{n} + \Delta t\mathbf{R}(\vec{\mathbf{W}}(t^{n+1})) = 0. \qquad [14]$$

The discrete form of equation [14] in time can be written in the following form,

$$\mathcal{F}((\mathcal{V}\vec{\mathbf{W}})^{n+1}, (\mathcal{V}\vec{\mathbf{W}})^{n}, \Delta t) = 0 \qquad [15]$$

where the flux calculated in the residual $\vec{\mathbf{R}}$ is evaluated at t^{n+1}. A combination of approximation and iterative methods are used to solve this non-linear system. The methods depend also on the type of spatial approximation chosen, as the evaluation (analytical, numerical or approximate finite differences) of the flux Jacobians is necessary. Both the structured and unstructured solvers considered here use the Van Leer FVS method for the spatial discretisation. The structured mesh solver from DLR uses an approximate factorisation implicit algorithm of Beam-Warming, [BEA 76], whereas the solvers from EPFL use a predictor-corrector multi-stage inexact Newton method. The outer loop is a recursive application of difference formula in time and the inner loops are non-linear and linear iterative solvers. As the characteristic time scales are small, explicit methods are still valid, especially when Runge-Kutta time

integration is performed. There is then a choice of updating within the intermediate time steps, as studied by Bendiksen, [BEN 97].

The implicit predictor-corrector method is now given. A multistep method is applied to the coupled system, [9], equivalent to a standard backward differencing scheme for a vector of variables $\vec{u}$ and a residual $R(\vec{u})$:

$$(1+\xi)\frac{\vec{u}^{n+1}-\vec{u}^{n}}{\Delta t}-\xi\frac{\vec{u}^{n}-\vec{u}^{n-1}}{\Delta t}=\theta R(\vec{u})^{n+1}-(1-\theta+\phi)R(\vec{u})^{n}-\phi R(\vec{u})^{n-1} \quad [16]$$

with parameters ξ, θ, ϕ depending on the operator splitting that is then introduced by the predictor-corrector phase, (see below) (usually $\xi = \phi = 0, \theta = \frac{1}{2}$, [BUT 87], [ROG 97]). R denotes again a residual.

Then for the nonlinear function of $(\vec{\mathbf{x}}, \vec{\mathbf{W}})$, the structure part and the fluid part must be taken at the same time level. The fluid part given by the system [15] can be constructed as the following :

– Predictor at t^*, $t^{n-1} < t^* < t^n$,

$$((\mathcal{V}\vec{\mathbf{W}})^*) - (\mathcal{V}\vec{\mathbf{W}})^{n-1}) = \theta R(\vec{\mathbf{W}})^* + (1-\theta)R(\vec{\mathbf{W}})^n, \theta \in [0,1]$$

– for the time steps t^{n-1}, t^*:

- do Newton iterations by
  - Initialise $(\mathcal{V}\vec{\mathbf{W}})^0$ by $(\mathcal{V}\vec{\mathbf{W}})^*$
  - At each Newton iteration k , do for $k : n-1 : *$, solve

$$\frac{\partial f((\mathcal{V}\vec{\mathbf{W}})^k)}{\partial \mathcal{V}\vec{\mathbf{W}}}\left((\mathcal{V}\vec{\mathbf{W}})^{k+1}-(\mathcal{V}\vec{\mathbf{W}})^k\right) = -f((\mathcal{V}\vec{\mathbf{W}})^k)$$

The initial approximation of the solution at time $t = t^0$ is calculated by a first-order time accurate implicit method. Then for the subsequent Newton iterations the following linear system has to be solved,

$$\left[I+\frac{\Delta t}{\mathcal{V}}\frac{\partial \vec{\mathbf{R}}(\mathbf{W})}{\partial \mathbf{W}}\bigg|_k\right]\left[(\mathcal{V}\mathbf{W})^{k+1}-(\mathcal{V}\mathbf{W})^k\right] = -\Delta t\vec{\mathbf{R}}(\mathbf{W}^k)) - \left[(\mathcal{V}\mathbf{W})^k-(\mathcal{V}\mathbf{W})^0\right] \quad [17]$$

– Corrector at time t^{n+1}, applying again the formula [16] between t^* and t^{n+1},

– do Newton at time step t^{n+1}

The linear subsystem in [17] is then resolved using the GMRES algorithm with no restarts and a small Krylov dimension. The Newton GMRES method is preconditioned by a diagonal preconditionner. At least two Newton iteration procedures must be performed per time step to ensure accuracy. The linear system is resolved until the L_2 norm of linear residual $||Ax - b||$ is converged to 10^{-2}.

The flux Jacobians are given by the $\partial\vec{\mathbf{R}}(\vec{\mathbf{W}})/\partial\vec{\mathbf{W}}$ term. These derivatives can be calculated exactly. The numerical scheme described above now also includes geometric quantities, which are time-dependent. The numerical flux evaluates the values across the cell interfaces, and hence the speed of the interface is incorporated. The enforcement of the discrete geometric conservation law, D-GCL, associated to the time scheme gives a measure of these geometrical terms. The modified consistency coefficients in expressions such as [16], and the mesh size need to be incorporated into the resulting scheme. The D-GCL arguments can be used for their evaluation, [FAR 98a]. The error analysis and the accuracy of the resulting time discretisation scheme depends also inherently upon these parameters.

The continuous GCL for the update of the volumes can be expressed as

$$\mathcal{V}^{n+1} - \mathcal{V}^n = -\int_{t^n}^{t^{n+1}} \left(\sum_{j \in v_i} \int_{\partial C_{ij}(t)} \vec{x}_t \cdot \vec{n} d\sigma \right) dt \qquad [18]$$

This equation states that the change in volume during the time integration from t^n to t^{n+1} has to be the same as the volume transpired through the cell faces. Therefore, the right hand side of [18] is called the transpiration flux. The discrete version, the D-GCL can use the same time integration scheme as the fluid solver.

4. Structural Solver

The Newmark method, [FAR 95], is used to integrate the structure's equation of motion :

$$[\mathbf{M}]\{\ddot{q}(t)\} + [\mathbf{K}]\{q(t)\} = \{\mathbf{F}(t)\} \qquad [19]$$

with acceleration, $\ddot{q}$, velocity $\dot{q}$ and and displacement q at time t^{n+1}, starting from a discrete initial condition, with airloads $\{F(t)\}$ at time step t^{n+1}. It can be considered as a generalisation of the constant average acceleration method.

The following approximations are used:

$$\begin{aligned} \dot{q}^{n+1} &= \dot{q}^n + \left[(1-\delta)\ddot{q}^n + \delta\ddot{q}^{n+1}\right]\Delta t \\ q^{n+1} &= q^n + \dot{q}^n\Delta t + \left[(\tfrac{1}{2}-\alpha)\ddot{q}^n + \alpha\ddot{q}^{n+1}\right]\Delta t^2 \end{aligned} \qquad [20]$$

The parameters ($\delta = 1/2, \alpha = 1/4$) give the constant average acceleration method and ($\delta = 1/2$, $\alpha = 1/6$) the linear acceleration method. The limit of unconditional stability of the Newmark method is given by $\beta \geq 1/4(\delta + 1/2)^2$, see Bathe [BAT 82]. Hence, the constant average acceleration method is unconditionally stable. Moreover, this method has no numerical dissipation which is very suitable for flutter calculations.

The complete system [9] now has to be solved combining the individual solvers fluid and structure in a fully coupled way. The goal is to devise techniques that integrate the fluid and the structure at the same time level and hence should preserve energy.

The equation of motion [19] is then solved for the acceleration $\ddot{q}^{n+1}$ with the airloads $\mathbf{F(t)}$ at t^{n+1}.

A time integration procedure then uses predicted displacements and corrected aerodynamic steps as discussed in the section 5.3.

5. Energy Conservation for Fluid-Structure Coupling Algorithms

Here fully coupled means that the fluid and the structural response are integrated in time as a closed system at the *same time level* by implicit methods; this is in contrast to the so called *staggered algorithms* whereby the fluid and the structure are integrated in time separately and the information transfer is done after every *update* time step. However since time steps as determined by [10] are very small, explicit methods evaluate at the same time level, as specifically designed staggered algorithms as shown in works of C. Farhat *et al.*, [FAR 95],[FAR 98b],[FAR 98c]. There exist several different methods of coupling the iterations between the fluid and the structure.

The coupling algorithm can be performed in a staggered way, with various degrees of subcycling of the fluid solver. These methods are often explicit and have stability constraints that can become inconsistent.

5.1. *Staggered Algorithms*

At time t^n the state of the fluid, structure and mesh is known. In order to advance the system to the next time level since the explicit fluid solver requires small time steps to maintain stability, whereas the structure solver often allows for larger time steps since its characteristic time scale is often larger, the fluid is subcycled according to the structure.

Standard staggered algorithm (Figure 2)

1. Predict the state of the structure at the end of the current time step ($t = t_s^{n+1}$).
2. Calculate the mesh movement during the current time step.
3. Integrate the fluid to the next time level t_f^{n+1} with as many time steps as needed for stability.
4. Update the structure to the next time level t_s^{n+1} using the fluid pressures on the boundary.

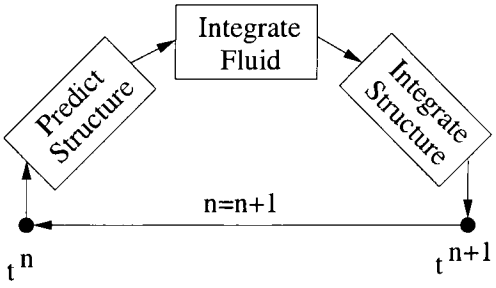

Figure 2. *Staggered coupling algorithm*

In this paper, more complex staggered algorithms are devised to overcome the time-lag and information loss. One of these methods is given in Figure 3, and is used together with the re-meshing method to solve the problems tackled here. Another is given in the Figure 5, and will be used in conjunction with the multistep inexact Newton method.

Corrected staggered algorithm (Figure 3)

1. Integrate structure from t_s^n to step $t = t_s^{n+1}$ using an intermediate prediction of the displacement
2. Extrapolate structural values and boundary position to $t = t_s^{n+1}$
3. Perform mesh movement
4. Integrate the fluid to the next time level, t_f^{n+1} calculate $\mathbf{F}$
5. Update the structure to the next time level corrected airloads.

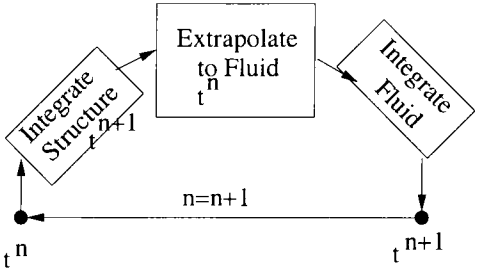

Figure 3. *A predicted-corrected staggered coupling algorithm*

Staggered methods introduce a time lag between the integration of fluid and structure. This means that the numerical problem which is solved is different from the physical problem which is modelled, and non-physical energy transfer is introduced in the system, as shown below, [MOU 96],[Le 96],[BLO 98c].

Indeed, the structure reacts to the aerodynamic forces and forces the flow to evolve with an interface speed, $\vec{V}_S$ which must be consistent, i.e. $\vec{V}_{mesh} = \vec{V}_{structure}$

$$\vec{V}_S{}^* = \frac{1}{2}(\dot{q}_s^{n+1} + \dot{q}_s^n) \qquad [21]$$

Typical predictions for the above algorithm are

$$\text{Prediction 1:} \quad \dot{q}_s^{n+1} = \dot{q}_s^n$$

$$\text{Prediction 2:} \quad \dot{q}_s^{n+1} = \dot{q}_s^n + \Delta t \ddot{q}_s^n$$

In the staggered approach the information transfer is not calculated at the same time (Prediction).

Using a consistent interface speed, i.e. when $\vec{V}^* = \frac{1}{2}(\dot{q}_s^{n+1} + \dot{q}_s^n)$ there will be no extra energy transfer.

An energy analysis is performed in order to assess the accuracy of the fluid-structure coupling algorithms. The energy which is transferred to the structure is given by the difference between the internal energy of the structure and the energy which is transferred from the fluid to the structure. When no energy is created or dissipated by the numerical coupling algorithm, this difference remains constant and equal to the initial internal energy of the structure. The total internal structural energy of the structure configuration (as for example the clamped wing or the blade assembly) is given by

$$W_i(t) = U(t) + T(t) = \frac{1}{2}\{q(t)\}^T[K]\{q(t)\} + \frac{1}{2}\{\dot{q}(t)\}^T[M]\{\dot{q}(t)\} \qquad [22]$$

where U is the strain energy and T is the kinetic energy of the structural system. The energy of the fluid submitted to or received from the structure (vibrating profile) is given by

$$W_e(t) = \int F(t) \cdot V_s(t) d\vec{x}$$

which for a vibrating profile can be given by

$$\approx \int_0^{\bar{h}(t)} -C_l d\bar{h} + \int_0^{\alpha(t)} C_m d\alpha \qquad [23]$$

where the integrals are usually calculated by the trapezoidal rule at $t^{n+1/2}$. The energy transferred to the structure is hence

$$W_s(t) = W_i(t) - W_e(t) \qquad [24]$$

Analytically, the transfer of energy over a period should be zero if there is no spurious energy production or dissipation within the system. The energy which is

transferred from the fluid to the structure per period is calculated by the integral of the product of the structural velocity and force which acts upon the structure,

$$E = \int_0^T \dot{q}_s(t) f(t) dt \qquad [25]$$

where $\dot{q}_s(t)$ is the structural velocity and $f(t)$ the external force. Assuming the forcing term and the displacement to be initially of the form

$$f(t) = \bar{f} cos(\omega t) \quad , \quad \dot{q}_s = \omega \bar{q}_s sin(\omega t) \qquad [26]$$

where $\bar{f}$ is the force amplitude and $\bar{q}_s$ is the amplitude of the displacement. Substitution of [26] in [25] gives,

$$E = \int_0^T \omega \bar{q}_s sin(\omega t) \bar{f} cos(\omega t) dt = 0 \qquad [27]$$

This shows that in the analytical case there is no net energy transfer between fluid and structure.

Using a staggered algorithm a time lag is introduced due to the fluid and structure interface velocity not being calculated at the same time. The force is now calculated at $t^{n+1} - \phi \Delta t$, where $0 \leq \phi < 1$ for the staggered schemes, which yields

$$E = \int_0^T \omega \bar{q}_s sin(\omega t) \bar{f} cos(\omega (t - \phi \Delta t)) dt = \omega \bar{q}_s \bar{f} sin(\omega \phi \Delta t) \frac{1}{2} T \qquad [28]$$

giving an energy source which transfers energy from the fluid to the structure when the pressure is calculated too early.

In order to avoid this effect, implicit fully coupled algorithms are devised, whereby the *update* occurs *at the same time level.* This energy analysis leads to the formulation of the Interaction Consistency Law (ICL). This law states that the time dependence of the boundary conditions of the separate solvers have to be consistent with the time integration of the solver which provides the boundary condition, [BLO 98b]. Accordingly the boundary conditions of both the fluid and structure contain the implicit variables of structure and fluid respectively. However, if the time steps are small, and the fluid CFL number is small, this discrepancy will hardly be noticeable, as shown within the results.

These remarks have also been proven mathematically in [Le 96],[Le 99].

Ideally the fluid-elastic mesh-structure should be integrated as a closed system, "monolithically", which means that the time integration of the fluid and the structure form a single discrete system, and are resolved implicitly. The interaction is performed then by the boundary conditions of the fluid and structure which are consistent with the discrete structure and fluid solvers respectively. This requires that the same numerical method be stable, non-dissipative and precise for each part, which is difficult

to achieve; for example: the Newmark method and its variants are unconditionnaly stable and robust for the deforming solid mechanics part, whereas this method creates unacceptable dissipation for the fluid part. Also such a matrix system will become too large to be conceivable in more than one or two dimensions with a low number of degrees of freedom, and cannot yet be conceived for multi-dimensional problems. Felker [FEL 93] constructed a monolithical solution algorithm for static fluid-structure interaction. Dynamic fluid-structure interaction contains an additional difficulty which is the influence of the time lag between fluid and structure which introduces non-physical energy dissipation into the system. Several authors as for example Alonso and Jameson [ALO 94], Melville *et al.* [MEL 97] and Morton *et al.* [MOR 97] have tackled these questions using either subiterative procedures or semi-closed system dynamics. Dynamic fluid-structure interaction involves time dependent information transfer from the fluid to the structure and vice versa. This information transfer only acts on the fluid-structure boundary. On the one hand the fluid pressures are transferred to the structure via the external force which acts on the structure. On the other hand the velocity of the mesh is equal to the velocity of the structure at the fluid-structure interface. In the staggered approach above, this information transfer is not calculated at the same time. For this algorithm a prediction of the structural velocity is transferred to the fluid. If this prediction were exact, there would be no extra energy transfer in the staggered algorithm, [PIP 95],[PIP 00]. In the monolithical approach this difference is zero by definition since the whole system is coupled by an implicit method. The idea of a monolithical algorithm is schematically shown in Figure 4. There is no time lag in the information transfer, since fluid and structure are enclosed in one system at every time step.

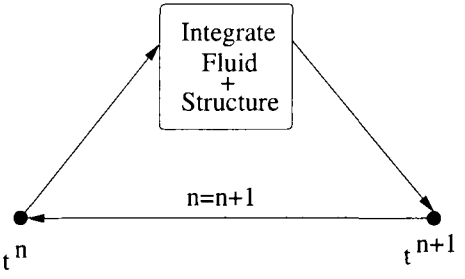

Figure 4. *Monolithical coupling algorithm*

5.2. *"Monolithical Coupling"*

A piston problem, where one single discrete operator containing the integration of the fluid, mesh, structure and interaction is applied at each time level to integrate the complete system in time has been studied by [PIP 95],[BLO 98b],[BLO 98c]. This piston problem is described by a one-dimensional equation for the fluid and a one degree of freedom system for the structure for which the exact expressions of the

matrices and the coupling matrices can be derived. Such a system has a matrix form as follows where the suffixes $_{f,s}$ denote fluid and structure respectively:

$$\begin{aligned}
[A_f]\left\{\mathbf{X}_f^{n+1}\right\} &= [B_f]\left\{\mathbf{X}_f^{n}\right\} + \{F_f\} \\
\text{with } \{F_f\} &= [Ca_{sf}]\left\{\mathbf{X}_s^{n+1}\right\} + [Cb_{sf}]\left\{\mathbf{X}_s^{n}\right\} + \left\{\bar{R}_f\right\} \\
[A_s]\left\{\mathbf{X}_s^{n+1}\right\} &= [B_s]\left\{\mathbf{X}_s^{n}\right\} + \{F_s\} \\
\text{with } \{F_s\} &= [Ca_{fs}]\left\{\mathbf{X}_f^{n+1}\right\} + [Cb_{fs}]\left\{\mathbf{X}_f^{n}\right\} + \left\{\bar{R}_s\right\}
\end{aligned} \qquad [29]$$

The source terms F_f and F_s are functions of $(\dot{q}_s)$ and (p_f). Ca_{sf} denotes the coupling matrix with implicit boundary velocity from the fluid equation, Ca_{fs} is the implicit forcing term for the structure, Cb_{sf}, Cb_{fs} are the counterparts of Ca_*. The force vectors $\bar{R}_f$ and $\bar{R}_s$ contain the boundary condition at the moving piston. As this system represents a one-dimensional problem it is possible to resolve these matrices as block tri-diagonal systems using Thomas-like algorithms, [BLO 98b], which cannot be extended to higher-dimensional problems.

It is hence quite obvious that such a method becomes rapidly unfeasible for more than one degree of freedom, and higher dimensional problems.

5.3. *Fully Coupled FSI Algorithms*

In order to develop an energy conserving method that is practicable for more complex problems, and be used for everyday realistic studies a compromise has be met. Farhat *et al.* in several papers, [FAR 98d],[FAR 00] as well as the present authors have hence turned towards strong coupling algorithms whereby several corrector steps are made iteratively to a staggered algorithm (structure is updated after the fluid integration) in such a way that the fluid, the mesh and the structure are integrated at the same time *level*:

The strong coupling algorithm applied here is obtained by applying several corrector steps to a staggered algorithm, in such a way that the structure is integrated at the same level as the fluid in time. The scheme is illustrated in Figure 5.

Fully coupled Predictor-Corrector algorithm

1. Predict the state of the structure at the end of the current time step ($t = t^{n+1}$).
2. Integrate the fluid to the next time level using the predicted state of the structure.
3. Update the structure to the next time level using the fluid pressures on the boundary.

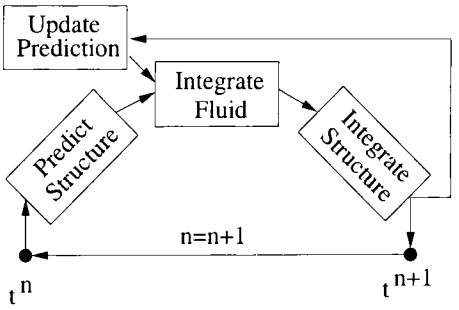

Figure 5. *Strongly Coupled Predictor-Corrector algorithm*

4. Restore all structure and fluid variables to t^n and return to step 2 with the current structural velocity $\dot{q}_s$ as an updated predicted state of the structure. This step is repeated several times before the system is moved on to the next time step.

These methods are now validated for a single stage aeroelastic NACA problem, and then a flutter response of a coupled compressor cascade.

6. Validation of Fully Coupling Techniques for an Aeroelastic NACA0012

In this section the fully coupled technique is applied to a more realistic text case: the aeroelastic behaviour of a NACA0012 airfoil supported by two linear springs.

The problem consists of a NACA0012 airfoil which is supported by two springs attached to the quarter chord. The configuration is shown in Figure 6, and is described also in [BAT 90],[FAR 90], [FAR 93],[RAU 89]. It is a generic problem of wing divergence: when an aircraft wing in flight is deformed, a moment is induced which will twist the wing. There will be a natural resistance by an elastic moment. The elastic stiffness is independent of the speed, whereas the aerodynamic moment is a direct function: a critical speed may be attained where the stiffness is just sufficient to bear the wing in a disturbed position. By considering a typical wing section supported by springs which represent the effect of the rotation α, around the elastic centre, with a torsion spring reacting to the pitching motion, and a linear spring reacting to the plunging motion with respect to the vertical displacement. Initially the airfoil is rotated through a small angle as a rigid body, Then this constraint is relaxed to let the wing deflect elastically through the angle α. The aerodynamic action is represented by the lift force L at the aerodynamic centre, and the pitching moment around the same point, M. For the NACA0012 this point can be approximated by the quarter chord length. When equilibrium is attained, the moment balances with the elastic restoring moment.

As the main forces for such an aeroelastic problem exerted on the structure are governed by the fluid pressure on the surface, it is sufficient to consider that the fluid flow is governed by the Euler equations.

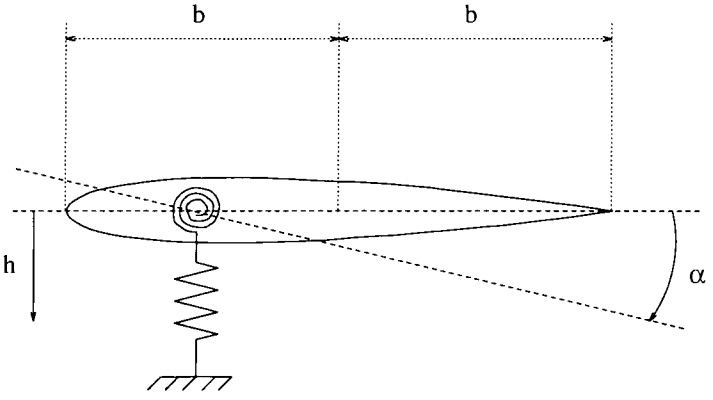

Figure 6. NACA0012 airfoil supported by springs

6.1. *Structural Model*

The structural model for the NACA0012 airfoil supported by two linear springs can be described by a two degrees of freedom equation for the aeroelastic structure of variables the pitching angle α and plunging displacement h. This is written first as the above general elastic system, [1], with the structural displacement

$$q_s \equiv \left\{ \begin{array}{c} \ddot{\bar{h}} \\ \\ \ddot{\alpha} \end{array} \right\} : \quad \begin{array}{lcl} m\ddot{h} + S_\alpha \ddot{\alpha} + \mathbf{K_h} \cdot h & = & L \\ \\ S_\alpha \ddot{h} + I_\alpha \ddot{\alpha} + \mathbf{K}_\alpha \cdot \alpha & = & M \end{array} \qquad [30]$$

Defining $\bar{h} = h/2b$, where b is the semi-chord (see Figure 6), m is the mass of the airfoil per unit span, S_α is the static moment around the elastic centre, I_α is the rotational moment of inertia.

The time is non-dimensionalised by taking the $\bar{t} = t \cdot U_\infty / 2b$. This can also be expressed in terms of the far field Mach number by choosing $\bar{t} = t \cdot a_\infty / 2b$, with a_∞ being the upstream speed of sound. The first expression corresponds to non-dimensionalising by the uncoupled natural frequency, $\bar{t} = t/\tau$, where $\tau = \omega_\alpha t$ and ω_h and ω_α are the decoupled natural frequencies of the plunging and pitching moment, respectively.

Taking

$$\mathbf{K}_\alpha = I_\alpha \omega_\alpha^2, \quad \mathbf{K_h} = I_\alpha \omega_h^2,$$

and introducing the reduced velocity $U^* = \frac{U_\infty}{\omega_\alpha \cdot b}$, then neglecting the damping term [30] can be written as

$$\begin{bmatrix} 1 & \frac{S_\alpha}{2mb} \\ \frac{S_\alpha}{2mb} & \frac{I_\alpha}{4mb^2} \end{bmatrix} \begin{Bmatrix} \ddot{\bar{h}} \\ \ddot{\alpha} \end{Bmatrix} + \begin{bmatrix} \frac{4t^* {\omega_h}^2}{U^{*2}\omega_\alpha^2} & 0 \\ 0 & \frac{t^* I_\alpha}{U^{*2} mb^2} \end{bmatrix} \begin{Bmatrix} \bar{h} \\ \alpha \end{Bmatrix} = \begin{Bmatrix} -\frac{2C_l t^*}{\pi\mu} \\ \frac{2C_m t^*}{\pi\mu} \end{Bmatrix} \quad [31]$$

where t^* represents a factor of M_∞^2 for the second choice of time scaling. C_l, C_m are the lift and moment coefficient, respectively. μ is the airfoil-air mass ratio defined by $\mu = m/\pi\rho b^2$. U^* is the non-dimensional velocity given by $U^* = U_\infty/b\omega_\alpha$. The double dot denotes a second order time derivative with respect to non-dimensional time $t^* = tU_\infty/L$.

The passage from one set of variables to the other can be done by adjusting the total values.

A choice of these non-dimensional values of these variables are given in Table 1. The velocity parameter U^* is varied in order to determine the stability limit.

Parameter	value	
ω_h	100	rad/s
ω_α	100	rad/s
S_α	0.9	kgm
m	1	kg
b	0.5	m
I_α	0.8695	kgm
μ	60	
M_∞	0.8	
γ	1.4	

Table 1. *Parameters for aeroelastic test case*

The following values of U^* are tested: 3.464, 5.447 and 6.928. The aeroelastic simulation is started after a perturbation of the airfoil angle by 0.01 radian. The reduced frequency is a measure for the unsteadiness of the flow and is calculated by $\omega^* = \frac{2\pi f L}{U_\infty}$, where f is the frequency of oscillation in Hertz, L is a reference length, here $L = 2b$, and U_∞ is the flow velocity at infinity. For the $U^* = 5.447$ value, the first and second eigenfrequency of the elastically supported airfoil are found to be $f_1 = 0.25$ Hz and $f_2 = 3.3 \times 10^{-2}$ Hz. The reduced frequencies which correspond to these eigenfrequencies are $\omega_1^* = 5.7 \times 10^{-3}$ and $\omega_2^* = 7.6 \times 10^{-4}$ are low, leading to

weak unsteady effects. The first value will show very slight damping effects, the last value will be more unsteady, (see Figure 9).

6.2. *Results for the NACA 0012 Aeroelastic Test Case*

Since for the first two values of U^* the unsteady effects are low, this reduces the number of outer Newton iterations necessary for the Predictor-Corrector method. At least two Newton iterations are performed per time step. The evolution of the angle and the plunging deflection is shown in Figures 7, 8, and 9 using the predictor-corrector staggered algorithm of Figure 3.

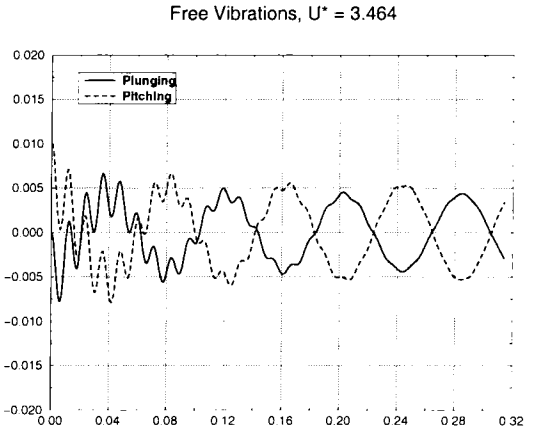

Figure 7. *Angle versus time. Pitching and Plunging deflection for the aeroelastic NACA;* $U^* = 3.464$.

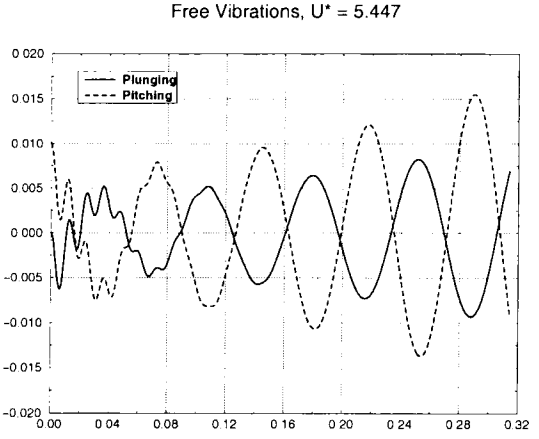

Figure 8. *Angle versus time. Pitching and Plunging deflection for the aeroelastic NACA;* $U^* = 5.447$.

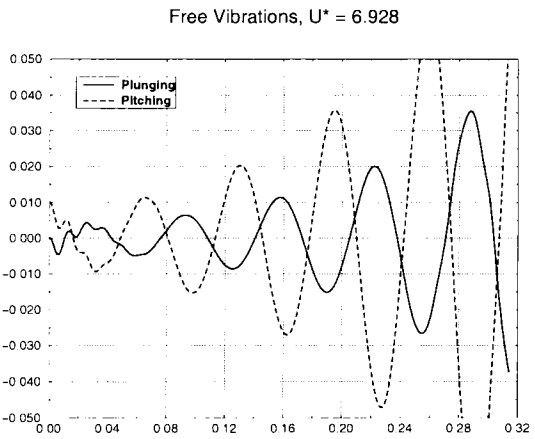

Figure 9. *Angle versus time. Pitching and Plunging deflection for the aeroelastic NACA; showing onset of instability for the higher reduced velocity case here,* $U^* = 6.928$.

In Figure 10 a comparison between the staggered algorithms with two different predictions of the structural state (zeroth and first order) of type Prediction 1 and Prediction 2 and the fully coupled implicit method is given for the case $U^* = 5.447$ for various CFL numbers.

For small CFL values the difference is weak. For higher values, the amplitude of the angle shows a deviation from the equilibrium zero angle position where the high frequency component of the structural vibration dominates the behaviour of the airfoil. The acceleration, which is used for the structural prediction, is less accurate for such high frequencies and large Δt and causes a shift downwards of the angular motion. This behaviour is not present in the strongly coupled algorithm which oscillates around the equilibrium position. For large time steps the high frequency component of the vibration does not damp out for the staggered algorithms.

The Energy dissipation is analysed in Figure 11 for the velocity parameter $U^* = 5.477$ which is just beyond the stability limit, [FAR 90]. The different methods: Staggered algorithm as in Figure 2, (prediction 1 and 2), and the Predictor-Corrector fully coupled are compared in the Figure 11. The CFL number is taken to be high, $CFL = 1200$. The figure shows clearly the energy creation of staggered methods, and the stabilising behaviour of the strongly coupled schemes. In the Figure 11, the Predictor-Corrector staggered algorithm is compared to the fully coupled one, (schemes of Figures 3 and 5) for the value $U^* = 5.477$. The difference is small, the unstable modes take longer to install with the fully implicit method, the methods can be considered to be equivalent from energy considerations. The $U^* = 6.928$ mode is clearly unstable.

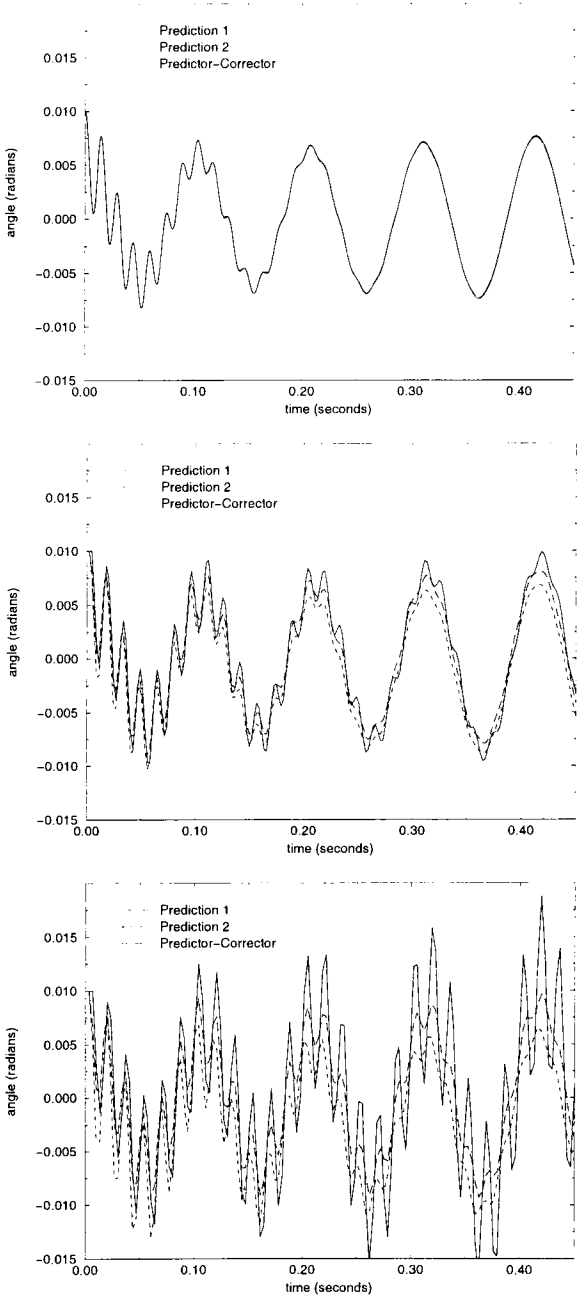

Figure 10. *Evolution of the angle for aeroelastic NACA0012, at at low CFL number, 100, CFL = 800 and CFL=1200 respectively, for the* $U^* = 5.447$ *case, using staggered, (Prediction 1 and 2) and strongly coupled Predictor-Corrector schemes*

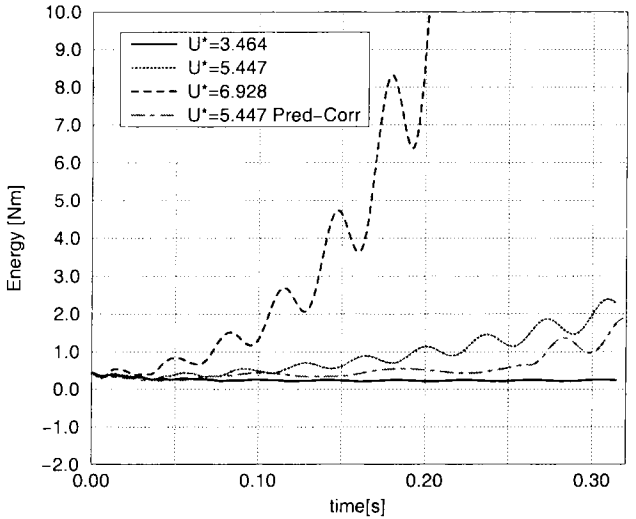

Comparisons between the staggered Predictor-Corrector scheme for different reduced velocity and the fully-coupled one at $U^* = 5.447$: the onset of unstable modes takes longer with the fully implicit method

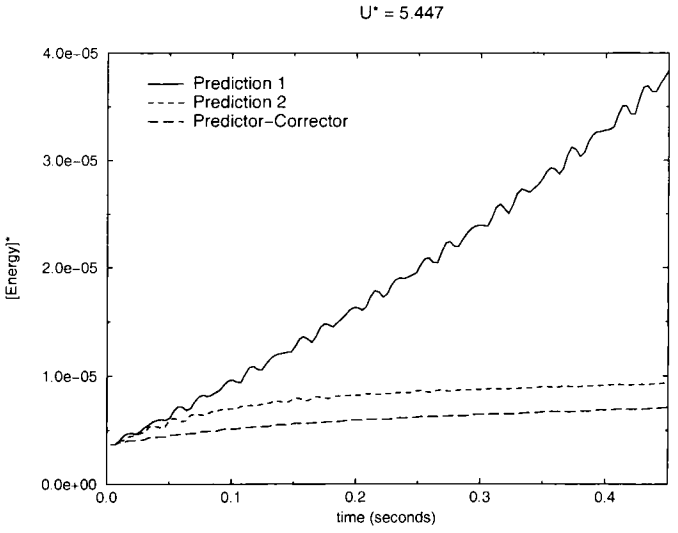

Figure 11. *Energy transfer for the aeroelastic NACA0012, at CFL=1000, comparison between staggered schemes, (Prediction 1, 2), and the fully coupled (Predictor-Corrector) scheme*

The aeroelastic motion is also calculated using another initial condition, taking the initial angular velocity to be $\dot{\alpha} = 0.01$ rad/s. The evolution of the angle calculated by two staggered algorithms and the fully coupled predictor-corrector algorithm is shown in Figure 12. The staggered algorithms are more sensitive to initial conditions. The qualitative behaviour of the fully coupled predictor-corrector algorithm remains uninfluenced by the change in initial conditions.

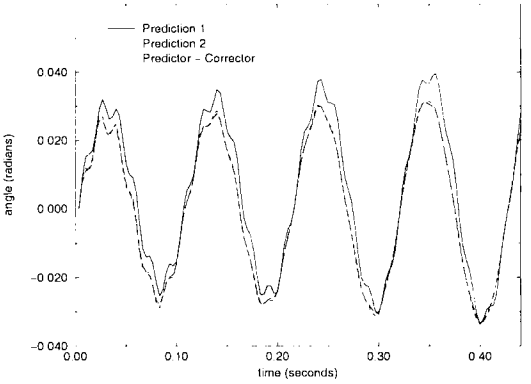

Figure 12. *Evolution of the angle for aeroelastic NACA0012, CFL=1200, for a change in the initial velocity condition*

6.3. *Limit Cycle Behaviour*

Increasing the reduced velocity U^* increases the possibility of unstable behaviour. The case of $U^* = 6.928$ has been shown to be unstable above. The simulation time now is extended here in time in order to find any non-linear behaviour. Both the structured mesh calculations at DLR and the unstructured mesh at EPFL were used to perform these analyses using the fully coupled predictor-corrector approach. The unstructured mesh consists of a 3693 nodes and 7266 elements triangular mesh. For the implicit multi-step Newton-GMRES algorithm, 4 to 5 subiterative sweeps were taken to ensure accuracy. This involves the evaluation of the diagonal and off-diagonal parts of a finite element type matrix which was extremely time consuming. Since the mesh deformation in this simulation is severe, the parameters of the spring analogy are changed with respect to the previous calculations, the segment springs are stiffened by a factor of five in one layer adjacent to the boundary. The semi-torsional improvement proposed by [TRA 98],[FAR 99],[BLO 99],[BLO 98a] is also applied. In these cases the structured elliptic re-meshing techniques have definitely an advantage.

The solutions with both methods are extremely similar. The evolution of the angle is shown in Figure 13 for a calculation up to 2.7 seconds. This limit cycle behaviour is even more apparent in the phase plot, Figure 13, where the angle velocity is plotted

against the angle. The curve follows a spiral and remains trapped in the limit cycle. This typical non-linear behaviour is also found by Kousen and Bendiksen [KOU 88] for the NACA64A006 airfoil supported by linear springs at transonic flow conditions using Runge-Kutta explicit methods, and in [BLO 98a] using a staggered algorithm.

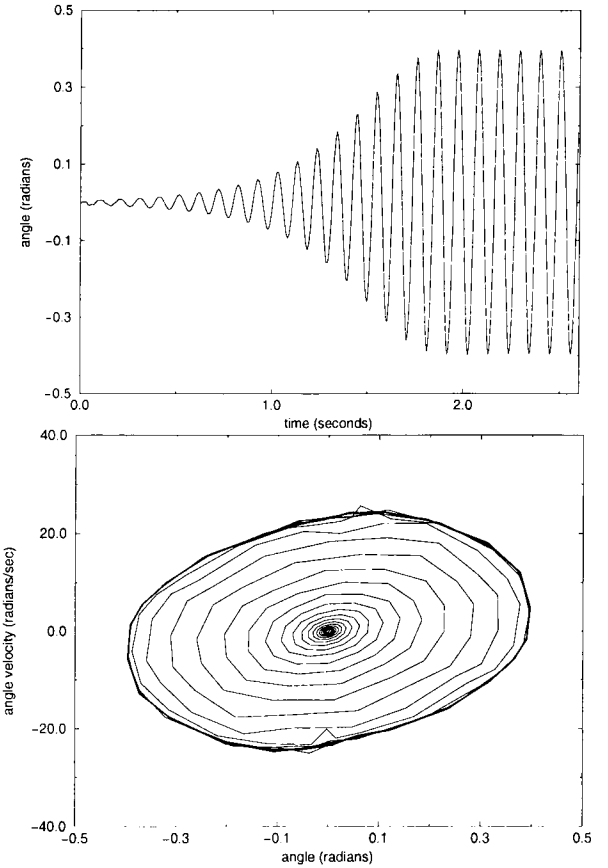

Figure 13. *Aeroelastic NACA0012: Time evolution of the angle, (top). Phase plot (below),* $U^* = 6.928$

The pressure distributions at several times during the simulation are shown in Figure 14. These figures show the very large shock motions which occur in this simulation. The shocks move back and forth from leading edge to trailing edge, changing from suction to pressure side. It is believed that the limit cycle is reached when the shock hits the trailing edge. This is visible in the solutions. When the shock reaches the trailing edge, the phase shift between the airfoil motion and the pressure response is eliminated. This phase shift is found to be responsible for flutter at transonic flow conditions by Isogai [ISO 79a],[ISO 79b],[ISO 80]. The physical principles of this phase shift can be found in [TIJ 77] and [TIJ 80].

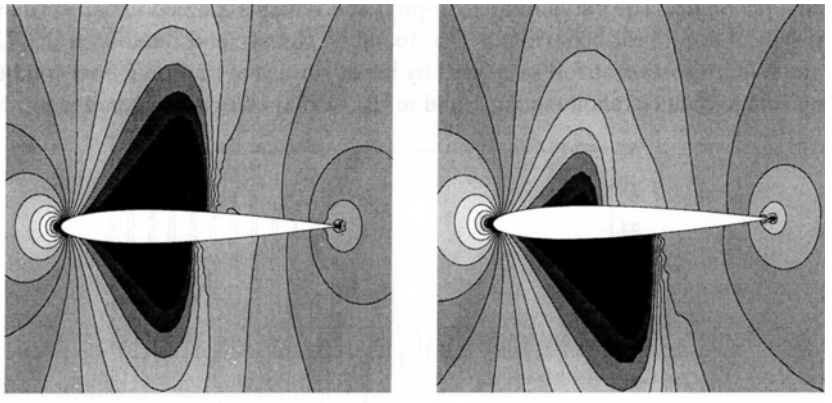

iso-pressure lines at t=0.23 and t=0.58

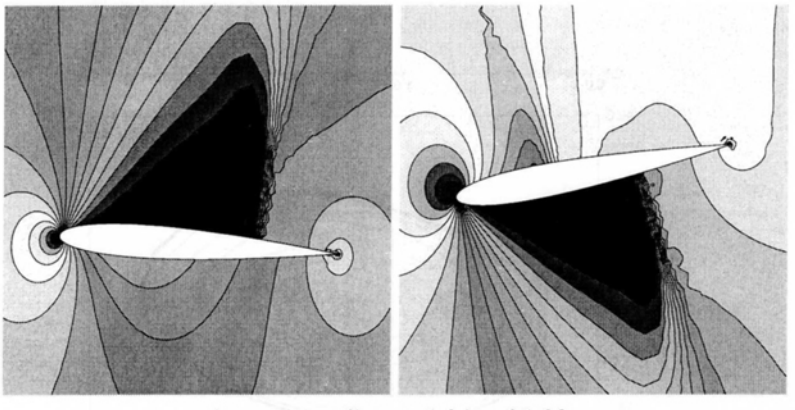

iso-pressure lines t=1.04 and 1.38

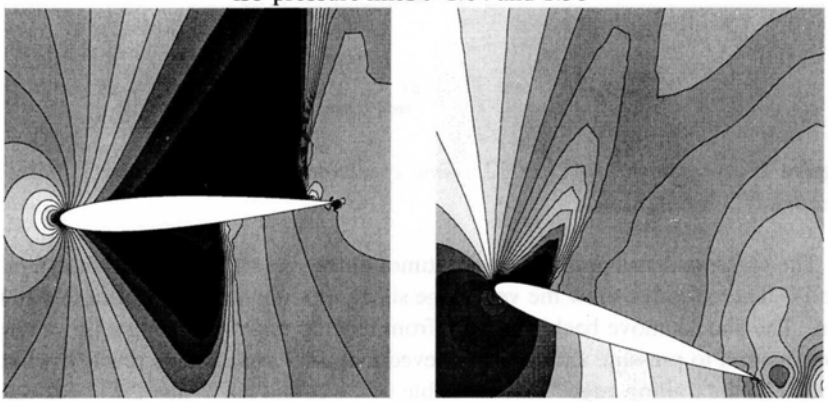

iso-pressure lines at t=2.10 and t=2.19

Figure 14. *Limit cycle motion of aeroelastic NACA0012 with the unstructured implicit solver,* $U^* = 6.928$

7. Flutter of the Direct Coupling of a Compressor Cascade

The main application of this paper is to study the non-linear flutter boundary of an oscillating compressor cascade, for which the blade to blade influence requires a direct coupled approach of the 20 blades. This study also allows insight into the aerodamping effects of tuning and mistuning, as related in the paper [CAR 00], and treats a complex realistic configuration. The compressor cascade is studied in high subsonic (inlet Mach number of 0.8) and transonic regime (inlet Mach number of 0.9), for which the linearised methods in the frequency domain are insufficient.

The 20 blade configuration corresponds to an annular test facility at LTT/EPFL, and consists of NACA3506 profile blades mounted on a mass-spring damper system, [BÖL 83],[KÖR 96]. These blades are mounted on torsional springs to simulate the torsional flexibility of the blades in a real cascade. This corresponds to a one degree of freedom model per blade. In order to evaluate the aeroelastic stability of the configuration, two different approaches are compared to each other: the forced vibration and the direct coupled approach. The forced vibration approach consists of performing several calculations where the blades are forced into one of the modes of the cascade at several frequencies. Since the cascade possesses 20 blades there are only 20 eigenmodes for the structural model chosen here. The aerodynamic stability of the modes at the corresponding frequency determines the stability of the configuration. Once theses modes have been identified, the direct approach consists of integrating the unsteady airloads together with the motion of the elastic mounted blades to simulate the vibration of the entire configuration.

The dynamic structural model is now written as a directly coupled system:

$$[\mathbf{M}]\{\ddot{\alpha}\} + [\mathbf{K}]\{\alpha\} = \{\mathbf{F}\} \qquad [32]$$

The damping term is considered here to be negligible; $\{\alpha\}$ is the vector of angular rotations of the blades, the structural mass and stiffness matrices $\mathbf{M}$ and $\mathbf{K}$ are diagonal:

$$\begin{bmatrix} I_\alpha & & 0 \\ & \ddots & \\ 0 & & I_\alpha \end{bmatrix} \begin{Bmatrix} \ddot{\alpha}_1 \\ \ddot{\alpha}_2 \\ \vdots \\ \ddot{\alpha}_{20} \end{Bmatrix} \begin{bmatrix} k_\alpha & & 0 \\ & \ddots & \\ 0 & & k_\alpha \end{bmatrix} \begin{Bmatrix} \alpha_1 \\ \alpha_2 \\ \vdots \\ \alpha_{20} \end{Bmatrix} = \begin{Bmatrix} \mathbf{M}_1 \\ \mathbf{M}_2 \\ \vdots \\ \mathbf{M}_{20} \end{Bmatrix} \qquad [33]$$

where k_α is the torsional stiffness and I_α is the rotational moment of inertia which is calculated by $I_\alpha = k_\alpha \omega^2$, where ω is the natural frequency of the blade/spring system.

The forces $\{\mathbf{F}\}$ contain the moments $\mathbf{M}_i$ of the individual blades i, the system is coupled via the aerodynamic coefficients.

The structural energy is given by

$$E = \frac{1}{2}\{\dot{\alpha}\}^T[\mathbf{M}]\{\dot{\alpha}\} + \frac{1}{2}\{\alpha\}^T[\mathbf{K}]\{\alpha\} \qquad [34]$$

The following parameters are taken for the calculations:

Total pressure (p_{t1})	2×10^5	Pa
Inlet speed of sound (c_1)	296	m/s
Torsional stiffness (k_α)	61.48	Nm/rad
Eigenfrequency case 1 (f_1)	184.6	Hz ($\omega^* = 0.4$)
Eigenfrequency case 2 (f_2)	92.3	Hz ($\omega^* = 0.2$)
Blade Type	NACA3506	
Number of Blades	20	
Blade Span (b)	0.04	m
Blade Chord (c)	0.08	m
Pitch (s)	0.0565	m
Stagger Angle (β_g)	40°	
Inflow Angle (β_1)	48.3°	
Ratio P_{st}/P_{tot} outlet β_p	0.81	

Table 2. *Geometrical parameters of cascade. The Inlet Mach numbers studied are* $M_1 = 0.8$ *and* 0.9

Two inlet Mach numbers are considered, $M_1 = 0.8$ and 0.9. The reduced frequency for the $M_1 = 0.8$ case is fixed at $\omega^* = 0.32$. The eigenmodes of the blades are characterised by the Inter-Blade Phase Angle (IBPA). To obtain the stability information of a configuration, forced vibration simulations are performed for a range of IBPA's. These simulations are performed at several frequencies around the corresponding structural eigenfrequencies. This provides the aerodynamic stability information of the configuration for a particular Mach number.

The computational domain is discretised for the EPFL code by an unstructured mesh around each blade with 94 nodes on the blade surface with 917 nodes and 1620 elements, repeated periodically as shown in Figure 15. Mesh movement uses the spring analogy, and the computational method uses the strongly coupled implicit method as described in the former section 5.3. For DLR, a structured mesh set up was employed using re-meshing with transfinite interpolation, (see the zoom in Figure 1), and a predicted staggered algorithm as described also in section 5.3.
The main concern will be the relative conservation of energy of the computational techniques for such a realistic test case.

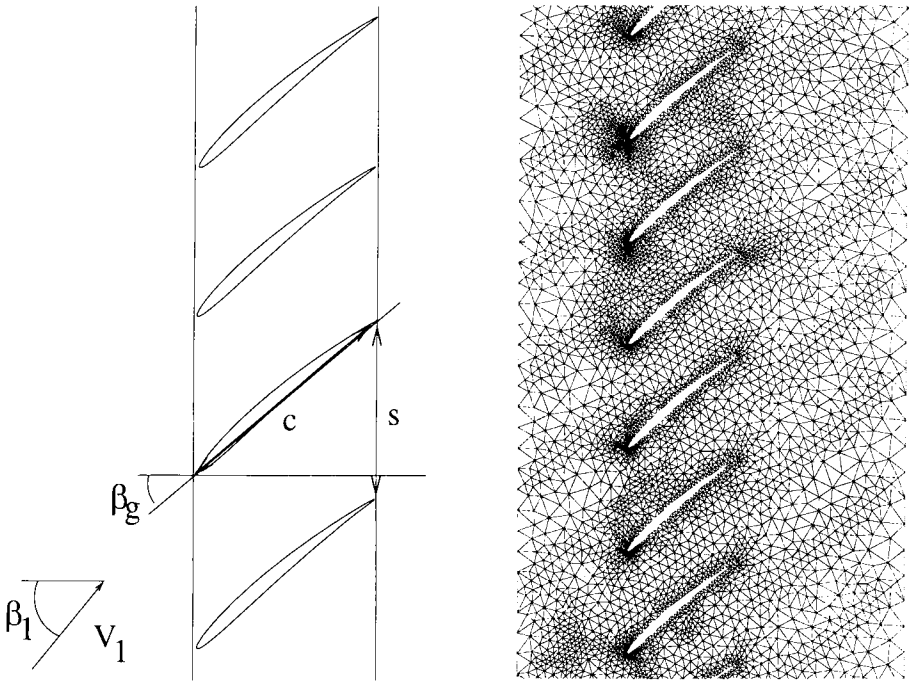

Figure 15. *Compressor cascade configuration and zoom on the unstructured computational mesh around several blades*

7.1. *Forced Vibration - Determination of the Unstable Modes (IBPA)*

7.1.1. *Aerodynamic Damping*

First, the calculation of the aerodynamic stability is discussed. Then the results of the numerical simulations are presented. These simulations are performed at several frequencies around the corresponding structural eigenfrequencies.

The Inter-Blade Phase Angle IBPA is given by

$$IBPA = \frac{2\pi k}{N}, \quad k = 1, ...N, \quad \text{N is the number of eigenvalues.}$$

The aerodynamic damping of the unsteady compressor cascade problem is given by the isolated forced vibration problem. For this simulation the cascade is excited in all its eigenmodes characterised by the Inter-Blade Phase Angle (IBPA). The simulation of all these interblade phase angles gives information about the aerodynamic damping of each mode. When the damping of one of these IBPA's is negative the cascade is unstable at that particular velocity.

The aerodynamic damping is calculated by means of the work Θ which is transferred from the fluid to the structure during one period of oscillation. The situation is stable when this power is negative. The power which is transferred from the fluid to the blade is given by

$$P(t) = \mathbf{M}(t)\dot{\alpha}(t) \qquad [35]$$

where $\mathbf{M}(t)$ is the unsteady moment and $\dot{\alpha}(t)$ the angle velocity of the blade.

$$\begin{aligned} \alpha(t) &= \alpha_0 + \bar{\alpha} sin(\omega t) \\ \dot{\alpha}(t) &= \frac{d\alpha(t)}{dt} = \bar{\alpha}\omega cos(\omega t) \\ \mathbf{M}(t) &= a_0 + \sum_{n=1}^{\infty} a_n cos(n\omega t) + b_n sin(n\omega t) \end{aligned} \qquad [36]$$

$\bar{\alpha}$ is the amplitude of the unsteady angle of attack. The steady offset of the angle of attack is denoted by α_0 and the frequency of oscillation is given by ω. The unsteady moment can be written as a Fourier series. Substitution of [36] in [35] gives

$$P(t) = \bar{\alpha} cos(\omega t) \left(a_0 + \sum_{n=1}^{\infty} a_n cos(n\omega t) + b_n sin(n\omega t) \right) \qquad [37]$$

The work transferred during a time lapse $t_1 - t_0$, is given by

$$\Theta = \int_{t_0}^{t_1} P(t)dt = \bar{\mathbf{M}}\bar{\alpha}\omega \int_{t_0}^{t_1} sin(\omega t + \varphi_m) cos(\omega t) dt \qquad [38]$$

Over a multiple of the period T of oscillation, the mean power is thus

$$\frac{\Theta}{T} = \frac{1}{2}\bar{\mathbf{M}}\bar{\alpha}\omega sin(\varphi_m) \qquad [39]$$

The transferred work hence only depends on the phase angle φ_m between the moment and angle.

The damping coefficient is defined as

$$\Xi = \frac{|\mathsf{C}_m|}{\bar{\alpha}} sin(\varphi_m) \qquad [40]$$

where the unsteady pitching moment C_m is given by

$$C_m = \frac{\mathbf{M}}{c(p_t - p_i)} \qquad [41]$$

where c is the chord length, p_t is the total pressure and p_i is the inlet pressure.

The damping coefficient is positive for unstable modes and negative for stable modes. The sign of the damping coefficient is opposite to that of the work Θ, a

decreasing value of Θ^n means that the cascade will be damped, and an increasing value means that the vibrations of the blades increase and flutter can occur.

The damping coefficient can be calculated by converging the Fourier series (which is slow) or by an equivalent hysteresis method from the C_m/α plot where the work is given by the area. Using equations [39] and [40] the relation between the aerodynamic damping Ξ and the work Θ is

$$\Xi = \frac{\Theta|C_m|}{\pi\bar{\alpha}^2\bar{\mathbf{M}}} \qquad [42]$$

An example of the estimation of the damping coefficient is given in Figure 16, for the IBPA=0° mode, where only one blade passage has to be simulated.

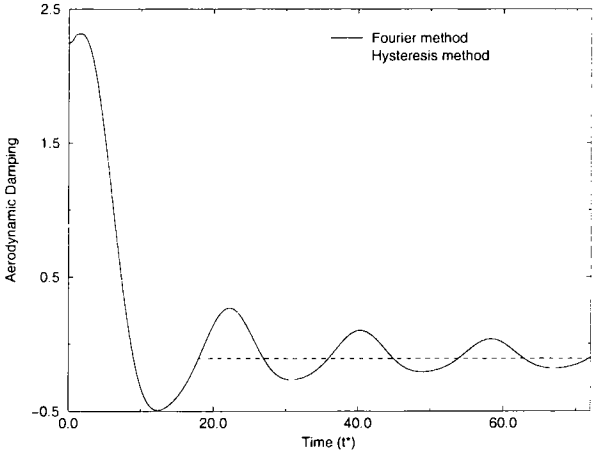

Figure 16. *Damping coefficient calculated with both the hysteresis and the Fourier series methods, for a reduced frequency of ω^*=0.35 in the $M_1 = 0.8$ case*

7.1.2. *Unstable mode detection*

The calculations are performed using the same techniques as in the previous section for the aeroelastic NACA0012, and the aerodynamic damping coefficients are calculated for different values of the IBPA. The damping coefficients Ξ are compared in Figure 17 for both the DLR and the EPFL calculations for Inter-Blade Phase Angles of $0°, 18°, 36°, 54°, 72°, 90°, 180°$ and $-90°$ for different values of the reduced frequency, ω^*. The most unstable eigenmode lies between 0° and 90°.

7.1.3. *Direct coupling of the whole assembly*

The dynamics of the system are given by Equation [32].

In order to evaluate the flutter boundary, first free blade vibrations are given. For this one blade is deflected initially for the $M_1 = 0.8$ conditions. The assembly becomes aeroelastically unstable, the flutter vibrations install after some time, with an

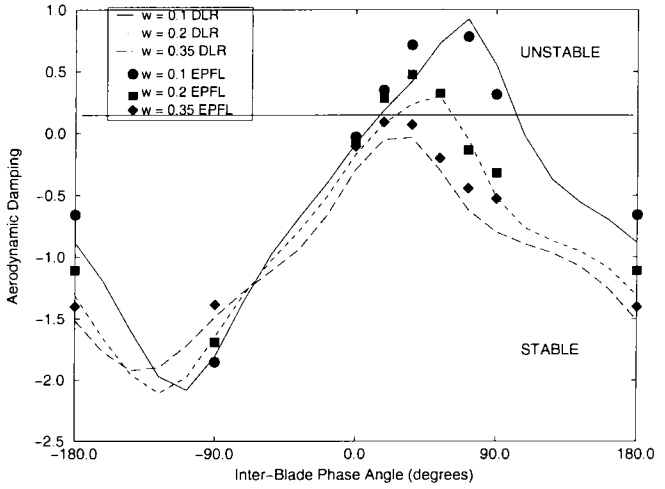

Figure 17. *Comparison of aerodynamic damping coefficients, search for the unstable modes,* $M_1 = 0.8$*, for different reduced frequencies in the range* $0.1 - 0.4$

almost constant IBPA between two blades, Figure 18. The time-series of three adjacent blades show the vibrations of blades 1 and 11 in phase, to an IBPA angle of 36^o. The system performs linearly in these conditions, (travelling wave solution).

Next we analyse for the $M_1 = 0.8$ case when the calculation is started by a forced vibration one. Here the calculation is started by perturbation of the angle in the first three eigenmodes $IBPA = 18°, 36°, 54°$ by 1/3 degree.

The amplitudes of all 20 blades are depicted in Figure 19 for the case of eigenfrequency 184.6 Hz. The stability of the configuration is difficult to deduce from this

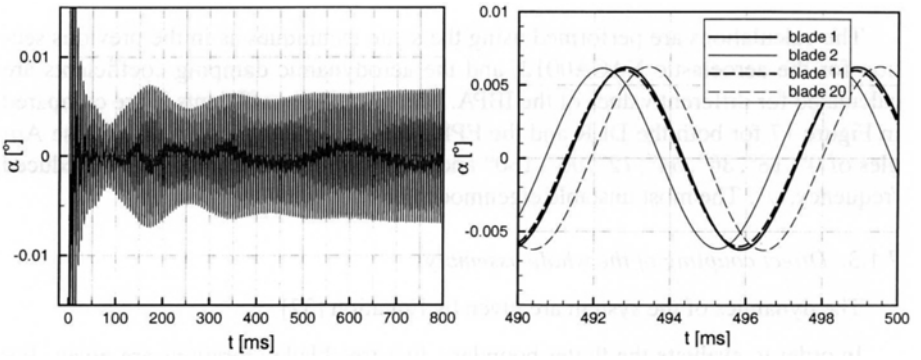

Figure 18. *Tuned cascade: free blade vibrations for* $M_1 = 0.8$*; Blade no. 1 at the left, and a zoom for adjacent blades which vibrate in phase, right*

figure. The structural energy is calculated and is superposed onto the figure for the free vibrations showing that the structural energy first decreases and then increases, Figure 21. This situation is hence weakly unstable. The decrease of the structural energy in the beginning of the simulation is caused by the vibration of the blades where all modes are present. Then the amplitude of the unstable IBPA's increases and the amplitude of the stable modes decreases. Then the blades start to vibrate in a more synchronised sense. This simulation is in agreement with the forced vibration calculation of before where two unstable IBPA's were also found. The mean frequency of the blades at the end of the simulation is 180.6 Hz. The flow around the blades has decreased the frequency of the blades by 2.2% from their natural frequency, which is 184.6 Hz. This is caused by an added mass effect of the flow to the blades. The blades have to deviate the flow when vibrating. By this deviation they displace the mass of the airflow which adds extra inertia to the blades. The stability information of the separate IBPA's, obtained by the forced vibration calculations in the previous section, is also reflected in the current direct coupled simulation. The interblade phase angle between the adjacent blades is also calculated for the direct coupled simulation, and are shown in Figure 20. The thick black lines are the $18°, 36°$ and $54°$ lines which serve as reference lines. The mean IBPA at the end of the simulation is situated under the $36°$ line and is still decreasing. This corresponds to the forced vibration calculation at $\omega_1^* = 0.4$, where the most unstable eigenmode is found at IBPA=18°.

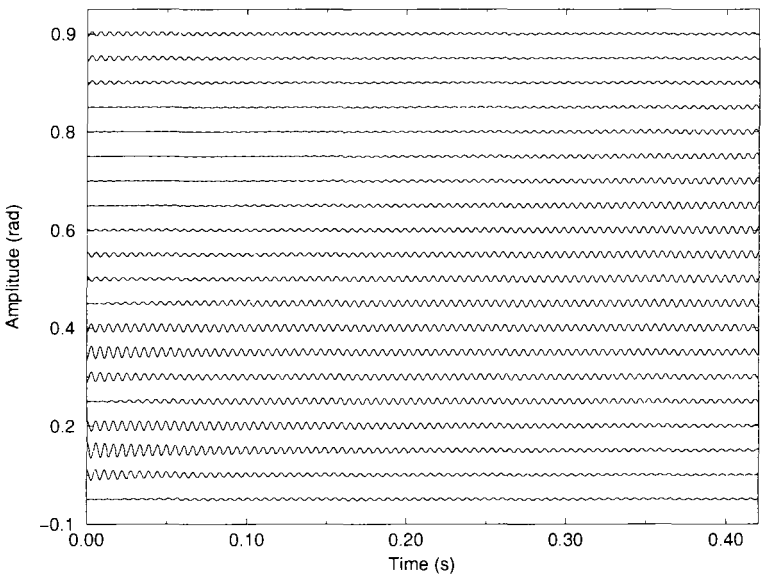

Figure 19. *Amplitude of the blade angles, direct coupling,* $f_1 = 184.6\ Hz$, $M_1 = 0.8$

Again the Figure 21 shows that the fully coupled method and the staggered predictor corrector method give equivalent energy preserving results for this realistic case,

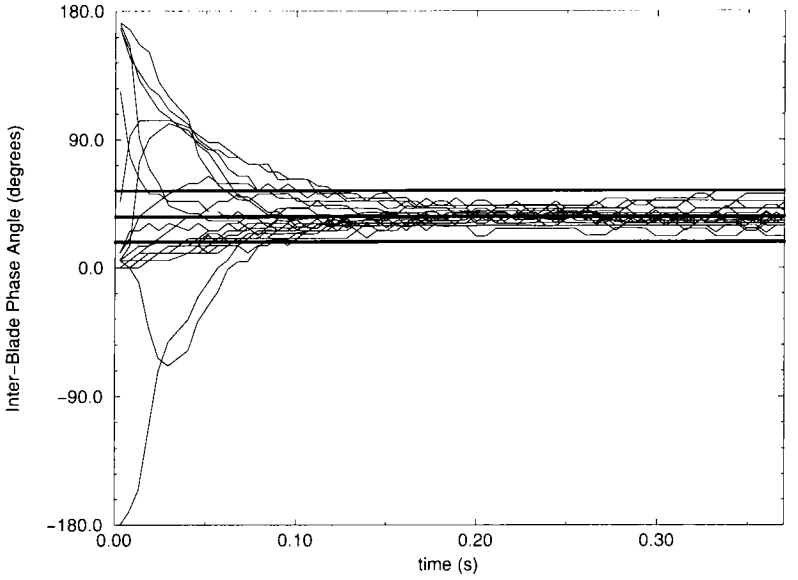

Figure 20. *IBPA of the blades, direct coupling,* $f_1 = 184.6$ *Hz, the thick lines represent the IBPA* 18°, 36° *and* 54°, $M_1 = 0.8$

as the fluid and the structure are evaluated at the same time level. The staggered method shows a deviation from the equilibrium position due to the spurious energy production/dissipation.

Next, the same analysis is made for the case of eigenfrequency 92.3 Hz. The amplitudes of all 20 blade angles are depicted in Figure 23. This is definitely an unstable case since the amplitudes of the blade angles increase during the time integration. This is also confirmed by Figure 22 which shows an exponential growth of the structural energy. The mean frequency of the blades at the end of the simulation is 90.3 Hz. Here the frequency is lowered by 2% which is caused again by the added mass effect. The convergence to a constant IBPA is more apparent for this case as can be seen in Figure 24. The mean IBPA is situated slightly above the 36° line. This corresponds to the forced vibration results where the 36° eigenmode is the most unstable one for the $\omega_2^* = 0.2$ case.

The solution fields are given in Figure 25, where one can see the iso-pressure lines for the mid-part of the cascade, and the relative change in the shock formation blade to blade.

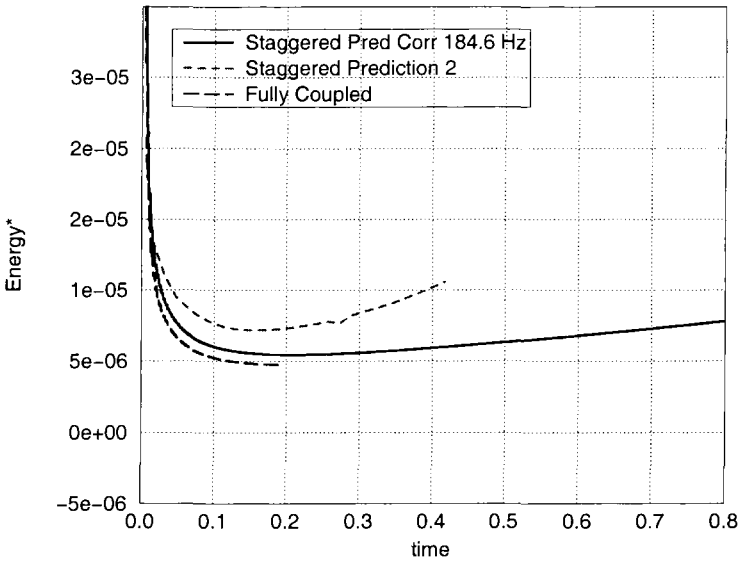

Figure 21. *Structural energy of the cascade for different schemes, direct coupling of the 20 blades,* $f_1 = 186.4\ Hz$ *(stable case)* $M_1 = 0.8$

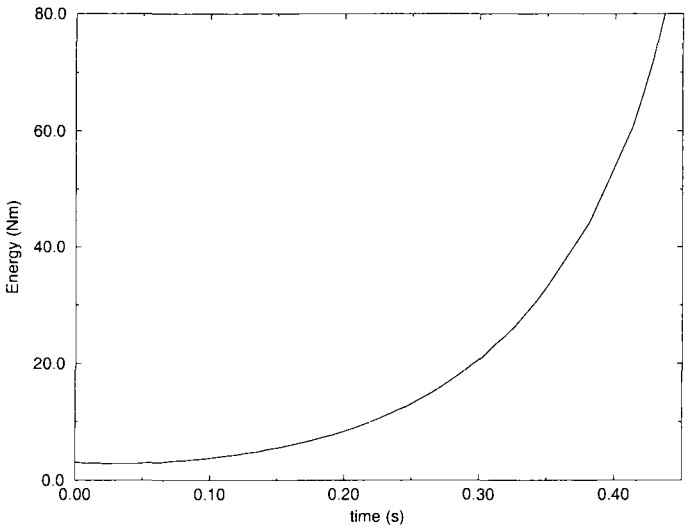

Figure 22. *Energy of the blades, direct coupling of the 20 blades with fully coupled scheme,* $f_2 = 92.3\ Hz$, $M_1 = 0.8$

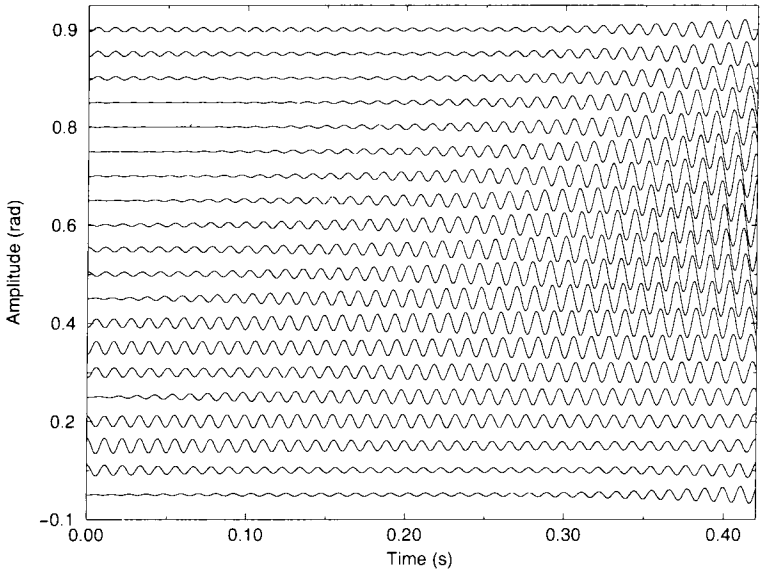

Figure 23. *Amplitude of the blade angles, direct coupling,* $f_2 = 92.3$ *Hz, (unstable),* $M_1 = 0.8$

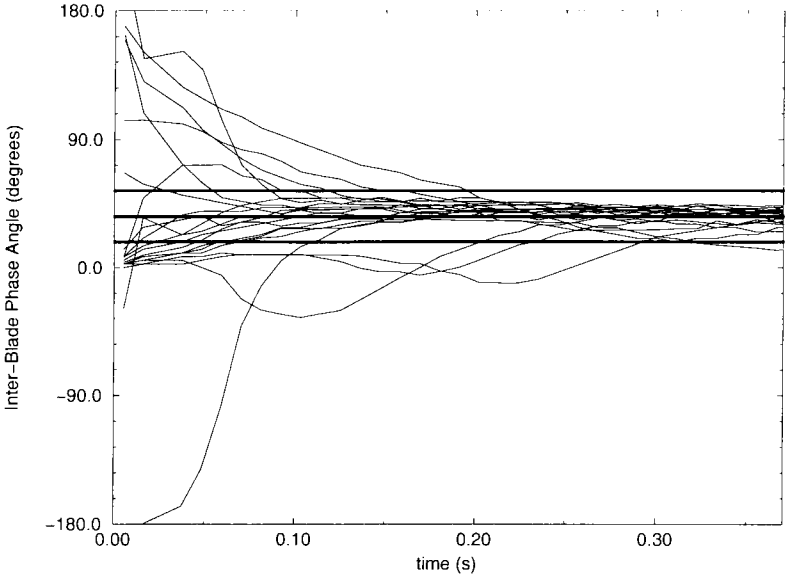

Figure 24. *IBPA of the blades, direct coupling,* $f_2 = 92.3$ *Hz, the thick lines represent the IBPA* $18°$, $36°$ *and* $54°$, $M_1 = 0.8$

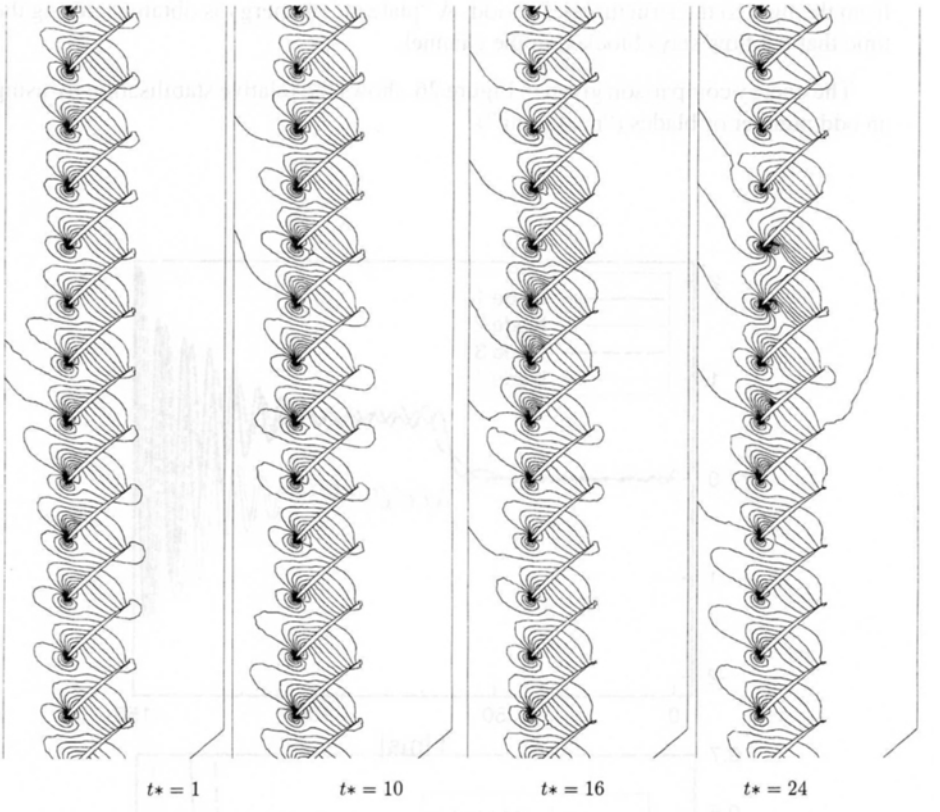

Figure 25. *Compressor cascade - Detail of the solutions at different instantaneous times*

7.2. *High Transonic Flow Conditions*

Lastly the higher inlet Mach number case is considered. Here the oscillating shocks within the blade channels lead to strong non-linear effects. The aeroelastic behaviour initially has the same characteristics as before, then there is a sharp change in the blade amplitudes due to the moving blade channel shock, which alters the average aerodynamic moment.

In Figure 26 the odd and even blades decouple, the odd blades go up and the even move down. Every other upstream blade channel acts as a nozzle, and this cannot happen in two adjacent rows. When the vibrations increase sufficiently, the channel becomes unchoked and flutter can appear. The most unstable IBPA mode is now 54^o.

An interesting effect is to compare the structural energy for 18, 19 or 20 blades calculated using the methods described above. For a 19 blade assembly, then the odd blades now go down and the even ones go up, there is hence less energy transferred

from the fluid to the structure per period. A "plateau" of energy is obtained during the time that the flow stays blocked in the channel.

The energy comparison given in Figure 26 shows the relative stabilisation by using an odd number of blades ("mistuning").

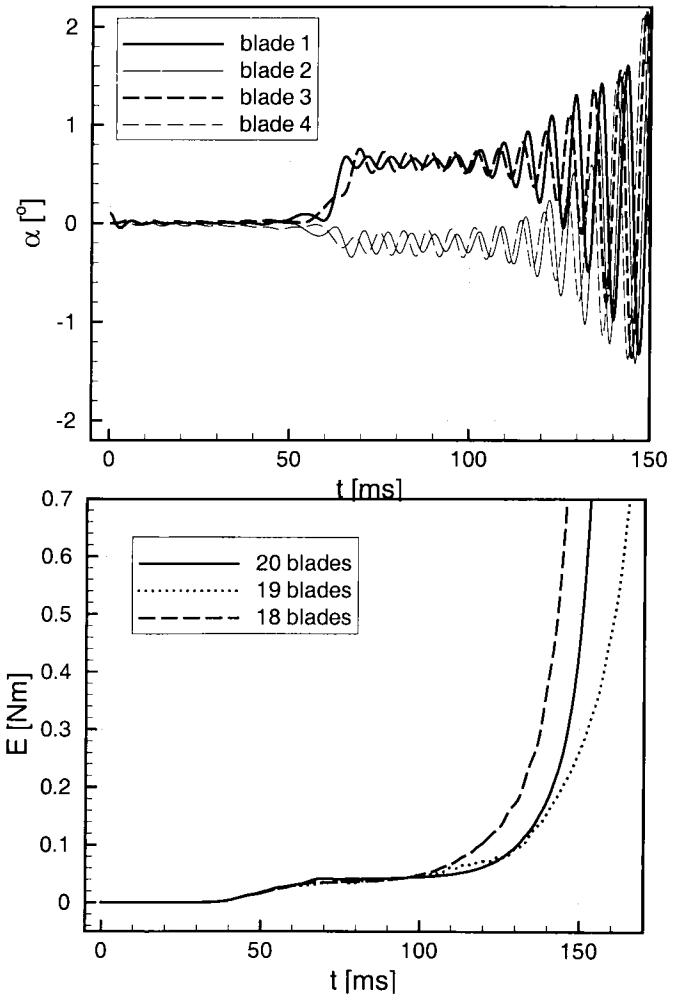

Figure 26. *Vibrations for high transonic flow conditions, $M_1 = 0.9$, showing the odd/even decoupling. Total structural energy of the cascade shows the unstable behaviour and the relative stabilisation by taking out one channel*

8. Conclusion

Strongly coupled fluid structure coupling techniques are applied to some realistic test cases. Energy considerations of the mechanical system gives insight into the accuracy of these methods for predicting instabilities. The importance of consistent boundary conditions, in space, on the interface boundary, within the spatial discretisation, and in time for the coupling method, have direct consequences on the energy prediction.

Only fully implicit strongly coupled algorithms where the coupling is performed at the same time level preserve the conservation of energy in the system.

Acknowledgements

The collaboration was made possible by the visiting scientist programme and the fellowship programme of the Leonhard Euler Centre, Swiss Pilot Centre of the European Research Community On Flow, Turbulence And Combustion (ERCOFTAC).

9. References

[ALO 94] ALONSO J., JAMESON A., "Fully-Implicit Time-Marching Aeroelastic Solutions", *AIAA Paper*, vol. 94-0056, 1994.

[BAT 82] BATHE K., *Finite Element Procedures in Engineering Analysis*, Prentice-Hall, Inc. New Jersey, 1982.

[BAT 90] BATINA J., "Unsteady Euler Airfoil Solutions Using Unstructured Dynamic Meshes", *AIAA Journal*, vol. 28, num. 8, 1990, p. 1381-1388.

[BEA 76] BEAM A., WARMING R. F., "An Implicit Finite-Differnece Algorithm for Hyperbolic Systems in Conservation Law Form", *Journal of Computational Physics*, vol. 22, 1976, p. 87-110.

[BEN 97] BENDIKSEN O., "Fluid-Structure Coupling Requirements for Time Accurate Aeroelastic Simulations", FREIDMANN P., PAÏDOUSSIS M., Eds., *AD-Vol. 53-3, 4^{th} International Symposium on Fluid-Structure Interaction, Aeroelasticity, Flow-Induced Vibrations and Noise*, vol. III, ASME, 1997.

[BLO 98a] BLOM F., *Investigations on Computational Fluid-Structure Interaction*, PhD thesis, Ecole Polytechnique Fédérale de Lausanne, No. 1865, 1998.

[BLO 98b] BLOM F., LEYLAND P., "Analysis of Fluid-Structure Interaction by Means of Dynamic Unstructured Meshes", *ASME Journal of Fluids Engineering*, vol. 120, 1998, p. 792-798.

[BLO 98c] BLOM F., LEYLAND P., "Consistency Analysis of Fluid-Structure Interaction Algorithms", *ECCOMAS 98*, John Wiley & Sons, Ltd., 1998.

[BLO 99] BLOM F., "Considerations on the Spring Analogy", *International Journal for Numerical Methods in Fluids*, vol. 14, 1999.

[BÖL 83] BÖLCS A., "A Test Facility for the Investigation of Steady and Unsteady Transonic Flows in Annular Cascades", *ASME Paper*, vol. GT, num. 34, 1983.

[BUT 87] BUTCHER J., *The Numerical Analysis of Ordinary Differential Equations*, John Wiley and Sons, Chichester, 1987.

[CAR 88] CARSTENS V., "Two-Dimensional Elliptic Grid Generation for Airfoils and Cascades", report num. DFVLR-FB 88-52, 1988, DLR.

[CAR 00] CARSTENS V., BELZ J., "Numerical Investigation of Nonlinear Fluid-Structure Interaction in Vibrating Compressor Blades", *ASME Turbo Expo 2000 Munich*, ASME, 2000.

[DON 82] DONEA J., GIULIANI S., HALLEUX J., "An Arbitrary Lagrangian-Eulerian Finite Element Method for Transient Dynamic Fluid-Structure Interactions", *Computer Methods in Applied Mechanics and Engineering*, vol. 33, 1982, p. 689-723.

[FAR 90] FARHAT C., LIN T., "Transient Aeroelastic Computations Using Multiple Moving Frames of Reference", *AIAA Paper*, vol. 90-3053, 1990.

[FAR 93] FARHAT C., LIN T., "A Structure Attached Corotational Fluid Grid For Transient Aeroelastic Computations", *AIAA Journal*, vol. 31, num. 3, 1993, p. 597-599.

[FAR 95] FARHAT C., "High Performance Simulation of Coupled Nonlinear Transient Aeroelastic Problems", Cosmase Course, EPF-Lausanne, 1995.

[FAR 98a] FARHAT C., *et al.*, "Invited Conference", *ECCOMAS Conference, Athens*, vol. II, 1998.

[FAR 98b] FARHAT C., LESOINNE M., "Higher-Order Staggered and Subiteration Free Algorithms for Coupled Dynamic Aeroelastic Problems", *AIAA Paper*, vol. 98-0516, 1998.

[FAR 98c] FARHAT C., LESOINNE M., LETALLEC P., "A Conservative Algorithm for Exchanging Aerodynamic and Elastodynamic Data in Aeroelastic Systems", *AIAA Paper*, vol. 98-0515, 1998.

[FAR 98d] FARHAT C., LESOINNE M., LETALLEC P., "Load and Motion Transfer Algorithms for Fluid/Structure Interaction Problems with Non-matching Discrete Interfaces: Momentum and Energy Conservation, Optimal Discretization and Application to Aeroelasticity", *Computer Methods in Applied Mechanics and Engineering*, vol. 157, 1998, p. 95-114.

[FAR 99] FARHAT C., DEGAND C., KOOBUS B., LESOINNE M., "Torsional Springs for Two-Dimensional Dynamic Unstructured Fluid Meshes", *Computer Methods in Applied Mechanics and Engineering*, vol. 163, 1999, p. 231-245.

[FAR 00] FARHAT C., LESOINNE M., "Two Efficient Staggered Procedures for the Serial and Parallel Solution of Three-Dimensional Nonlinear Transient Aeroelastic Problems", *Computer Methods in Applied Mechanics and Engineering*, vol. 182, 2000, p. 499-516.

[FEL 93] FELKER F., "Direct Solution of Two-Dimensional Navier-Stokes Equations for Static Aeroelasticity Problems", *AIAA Journal*, vol. 31, num. 1, 1993, p. 148-153.

[GRÜ 96] GRÜBER B., CARSTENS V., "Computation of the Unsteady Transonic Flow in Harmonically Oscillating Turbine Cascades Taking into Account Viscous Effects", *ASME Journal of Turbomachinery*, vol. 120, num. 1, 1996, p. 104-111.

[ISO 79a] ISOGAI K., "On the Transonic-Dip Mechanism of Flutter of a Sweptback Wing", *AIAA Journal*, vol. 17, num. 7, 1979, p. 793-795.

[ISO 79b] ISOGAI K., "On the Transonic-Dip Mechanism of Flutter of a Sweptback Wing: Part II", *AIAA Journal*, vol. 19, num. 9, 1979, p. 1240-1242.

[ISO 80] ISOGAI K., "Numerical Study of a Two-Dimensional Airfoil", report num. TR-617T, 1980, National Aerospace Laboratory, Japan.

[KÖR 96] KÖRBACHER H., BÖLCS A., "Steady-State and Time-Dependent Experimental Results of a NACA-3506 Cascade in an Annular Channal", *ASME Paper*, vol. GT-334, ASME, 1996.

[KOU 88] KOUSEN K., BENDIKSEN O., "Nonlinear Aspects of the Transonic Aeroelastic Stability Problem", *AIAA Paper*, vol. 88-2306, 1988.

[Le 96] LE TALLEC P., MOURO J., "Structures en Grands Deplacements couplées à des fluides en mouvement", report num. RR-2961, 1996, INRIA.

[Le 99] LE TALLEC P., MANI S., "Conservation Laws for Fluid-Structure Interactions", *International Symposium Computational Methods for Fluid-Structure Interaction, Trondheim, Norway*, Tapir Forlag, 1999.

[MEL 97] MELVILLE R., MORTON S., RIZZETTA D., "Implementation of a Fully-Implicit Aeroelastic Navier-Stokes Solver", *AIAA Paper*, vol. 97-2039, 1997.

[MOR 97] MORTON S., MELVILLE R., VISBAL M., "Accuracy and Coupling Issues of Aeroelastic Navier-Stokes Solutions on Deforming Meshes", *AIAA Paper*, vol. 97-1085, 1997.

[MOU 96] MOURO J., "Interactions Fluide Structure en Grands Déplacements, Résolution Numérique et Application aux Composants Hydrauliques Automobiles", PhD thesis, Ecole Polytechnique, France, 1996.

[PIP 95] PIPERNO S., "Simulation Numérique de Phénomènes d'Interaction Fluide-Structure", PhD thesis, Ecole Nationale Des Ponts et Chaussées, France, 1995.

[PIP 00] PIPERNO S., FARHAT C., "Design of Efficient Partitioned Procedures for the Transient Solution of Aeroelastic Problems", *Revue Européenne des Eléments Finis*, vol. this issue, 2000.

[RAU 89] RAUSCH R., BATINA J., YANG H., "Euler Flutter Analysis of Airfoils Using Unstructured Dynamic Meshes", *AIAA Paper*, vol. 89-1384, 1989.

[ROG 97] ROGIEST P., "An Implicit Finite Volume Scheme for the Computation of Unsteady Compressible Flows", PhD thesis, Von Karman Institute, 1997.

[TIJ 77] TIJDEMAN H., "Investigations of the Transonic Flow Around Oscillating Airfoils", PhD thesis, Technical University of Delft, The Netherlands, 1977.

[TIJ 80] TIJDEMAN H., SEEBASS R., "Transonic Flow Past Oscillating Airfoils", *Annual Review of Fluid Mechanics*, vol. 12, 1980, p. 181-222.

[TRA 98] TRAN H., KOOBUS B., FARHAT C., "Numerical Solution of Vortex Dominated Flow Problems with Moving Grids", *AIAA Paper*, vol. 98-0766, 1998.